

# Secrets of GrabCut and Kernel K-means

Meng Tang

Ismail Ben Ayed

Dmitrii Marin

Yuri Boykov

University of Western Ontario (UWO), Canada

mtang73@csd.uwo.ca

ibenayed@uwo.ca

dmitry.marin@gmail.com

yuri@csd.uwo.ca

## Abstract

The log-likelihood energy term in popular model-fitting segmentation methods, e.g. [64, 14, 50, 20], is presented as a generalized “probabilistic” K-means energy [33] for color space clustering. This interpretation reveals some limitations, e.g. over-fitting. We propose an alternative approach to color clustering using kernel K-means energy with well-known properties such as non-linear separation and scalability to higher-dimensional feature spaces. Similarly to log-likelihoods, our kernel energy term for color space clustering can be combined with image grid regularization, e.g. boundary smoothness, and minimized using (pseudo-) bound optimization and max-flow algorithm. Unlike histogram or GMM fitting [64, 50] and implicit entropy minimization [20], our approach is closely related to general pairwise clustering such as average association and normalized cut. But, in contrast to previous pairwise clustering algorithms, our approach can incorporate any standard geometric regularization in the image domain. We analyze extreme cases for kernel bandwidth (e.g. Gini bias) and propose adaptive strategies. Our general kernel-based approach opens the door for many extensions/applications.

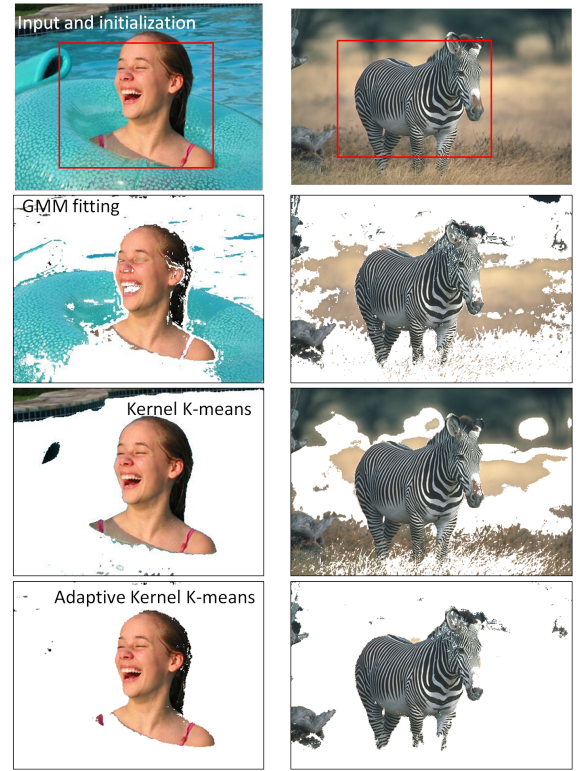


Figure 1: Failure of iterative GMM fitting *without* image smoothness or hard constraints. Our proposed kernel K-means & adaptive kernel K-means find better color clusters.

## 1. Introduction and Motivation

Many standard segmentation methods combine regularization in the image domain with a likelihood term integrating color appearance models [7, 64, 14, 9, 50]. These appearance models are often treated as variables and estimated jointly with segmentation by minimizing energies like

$$- \sum_{i=0}^{K-1} \sum_{p \in S^i} \log P^i(I_p) + ||\partial S|| \quad (1)$$

where segmentation  $\{S^i\}$  is defined by integer variables  $S_p$  such that  $S^i = \{p : S_p = i\}$ , models  $P = \{P^i\}$  are probability distributions of a given class, and  $||\partial S||$  is the segmentation boundary length in Euclidean or some contrast sensitive image-weighted metric. This popular approach to

unsupervised [64, 14] or supervised [50] segmentation combines smoothness or edge detection in the image domain with the color space clustering by *probabilistic K-means* [33], as explained later. The goal of this paper is to replace standard likelihoods in regularization energies like (1) with a new general term for clustering data points  $\{I_p | p \in \Omega\}$  in the color space based on *kernel K-means*.

Our methodology is general and applies to multi-label segmentation problems. For simplicity, our presentation is limited to a binary case  $K = 2$  where  $S_p \in \{0, 1\}$ . We use  $S = S^1$  and  $\bar{S} = S^0$  to denote two segments.



| A. basic K-means <sup>1</sup> (e.g. [14])   |  |
|---|--|
| $\sum_{p \in \mathbf{S}} \ I_p - \mu_{\mathbf{s}}\ ^2 + \sum_{p \in \bar{\mathbf{S}}} \ I_p - \mu_{\bar{\mathbf{s}}}\ ^2$ $= \frac{\sum_{pq \in \mathbf{S}} \ I_p - I_q\ ^2}{2 \mathbf{S} } + \frac{\sum_{pq \in \bar{\mathbf{S}}} \ I_p - I_q\ ^2}{2 \bar{\mathbf{S}} }$ $\stackrel{c}{=} -\sum_{p \in \mathbf{S}} \ln \mathcal{N}(I_p   \mu_{\mathbf{s}}) - \sum_{p \in \bar{\mathbf{S}}} \ln \mathcal{N}(I_p   \mu_{\bar{\mathbf{s}}})$  | <b>Variance criterion</b><br>$=  \mathbf{S}  \cdot \text{var}(\mathbf{S}) +  \bar{\mathbf{S}}  \cdot \text{var}(\bar{\mathbf{S}})$   |
|  more complex probability models   |  more complex data representation   |
| B. probabilistic K-means (e.g. [64, 55, 51, 50, 20])  | C. kernel K-means (ours)   |
| <p>(i) equivalent energy formulations:</p> $\sum_{p \in \mathbf{S}} \ I_p - \theta_{\mathbf{s}}\ _d + \sum_{p \in \bar{\mathbf{S}}} \ I_p - \theta_{\bar{\mathbf{s}}}\ _d$ $= -\sum_{p \in \mathbf{S}} \ln \mathcal{P}(I_p   \theta_{\mathbf{s}}) - \sum_{p \in \bar{\mathbf{S}}} \ln \mathcal{P}(I_p   \theta_{\bar{\mathbf{s}}})$   | <p>(i) equivalent energy formulations:</p> $\sum_{p \in \mathbf{S}} \ \phi(I_p) - \mu_{\mathbf{s}}\ ^2 + \sum_{p \in \bar{\mathbf{S}}} \ \phi(I_p) - \mu_{\bar{\mathbf{s}}}\ ^2$ $= \frac{\sum_{pq \in \mathbf{S}} \ \phi(I_p) - \phi(I_q)\ _k^2}{2 \mathbf{S} } + \frac{\sum_{pq \in \bar{\mathbf{S}}} \ \phi(I_p) - \phi(I_q)\ _k^2}{2 \bar{\mathbf{S}} }$ $\stackrel{c}{=} -\frac{\sum_{pq \in \mathbf{S}} k(I_p, I_q)}{ \mathbf{S} } - \frac{\sum_{pq \in \bar{\mathbf{S}}} k(I_p, I_q)}{ \bar{\mathbf{S}} }$  |
| <p>(ii) example: descriptive models (histograms or GMM) yield high-order log-likelihood energy</p> $-\sum_{p \in \mathbf{S}} \ln \mathcal{P}_h(I_p   \mathbf{S}) - \sum_{p \in \bar{\mathbf{S}}} \ln \mathcal{P}_h(I_p   \bar{\mathbf{S}})$ $\approx  \mathbf{S}  \cdot H(\mathbf{S}) +  \bar{\mathbf{S}}  \cdot H(\bar{\mathbf{S}}) \quad \textbf{Entropy criterion}$ <p><small>this approximation is valid only for highly descriptive models</small></p> <p><math>\mathcal{P}_h(\mathbf{S}) \equiv \mathcal{P}_h(\cdot   \mathbf{S})</math> - histogram (or GMM) for intensities in <math>\mathbf{S}</math><br/> <math>H(\mathbf{S})</math> - entropy for intensities in <math>\mathbf{S}</math></p> | <p>(ii) example: normalized kernels (Gaussians) yield high-order Parzen density energy</p> $-\sum_{p \in \mathbf{S}} \mathcal{P}_k(I_p   \mathbf{S}) - \sum_{p \in \bar{\mathbf{S}}} \mathcal{P}_k(I_p   \bar{\mathbf{S}})$ $\stackrel{c}{\approx}  \mathbf{S}  \cdot G(\mathbf{S}) +  \bar{\mathbf{S}}  \cdot G(\bar{\mathbf{S}}) \quad \textbf{Gini criterion}$ <p><small>this approximation is valid only for small-width normalized kernels<sup>2</sup></small></p> <p><math>\mathcal{P}_k(\mathbf{S}) \equiv \mathcal{P}_k(\cdot   \mathbf{S})</math> - kernel (Parzen) density for intensities in <math>\mathbf{S}</math><br/> <math>G(\mathbf{S})</math> - Gini impurity for intensities in <math>\mathbf{S}</math></p> |
| <p>(iii) bound optimization: auxiliary function at <math>\mathbf{S}^t</math></p> $A_t(\mathbf{S}) = -\sum_{p \in \mathbf{S}} \ln \mathcal{P}_h(I_p   \mathbf{S}^t) - \sum_{p \in \bar{\mathbf{S}}} \ln \mathcal{P}_h(I_p   \bar{\mathbf{S}}^t)$ $=  \mathbf{S}  \cdot H(\mathbf{S}   \mathbf{S}^t) +  \bar{\mathbf{S}}  \cdot H(\bar{\mathbf{S}}   \bar{\mathbf{S}}^t)$   | <p>(iii) bound optimization: auxiliary function at <math>\mathbf{S}^t</math></p> $A_t(\mathbf{S}) \approx -2 \sum_{p \in \mathbf{S}} \mathcal{P}_k(I_p   \mathbf{S}^t) - 2 \sum_{p \in \bar{\mathbf{S}}} \mathcal{P}_k(I_p   \bar{\mathbf{S}}^t)$ $+  \mathbf{S}  \cdot [G(\bar{\mathbf{S}}^t) - G(\mathbf{S}^t)]$   |

Table 1: *K-means terms for color clustering* that can be combined with Potts model for the segmentation boundary, e.g. (1). Basic K-means (A) corresponds to Gaussian model fitting minimizing cluster variances. Fitting more complex models like elliptic Gaussian [55, 51, 20], gamma/exponential distributions [2], GMM or histograms [64, 50] corresponds to *probabilistic K-means* (B), see [33]. Instead, we propose *kernel K-means* approach (C) using more complex data representation.

### 1.1. Probabilistic K-means (pKM)

The connection of the likelihood term in (1) to K-means clustering is obvious in the context of Chan-Vese approach [14] where probability models  $P$  are Gaussian with fixed variances. In this case, the likelihoods in (1) reduce to

$$\sum_{p \in \mathbf{S}} \|I_p - \mu_{\mathbf{s}}\|^2 + \sum_{p \in \bar{\mathbf{S}}} \|I_p - \mu_{\bar{\mathbf{s}}}\|^2 \quad (2)$$

the sum of squared errors from each cluster mean. This is the standard K-means objective for clustering, Table 1A.

One way to generalize Chan-Vese’s color clustering is to replace squared Euclidean distance in (2) by other *distortion*

measures  $\|\cdot\|_d$  corresponding to a general *distortion energy*

$$\sum_{p \in \mathbf{S}} \|I_p - \mu_{\mathbf{s}}\|_d + \sum_{p \in \bar{\mathbf{S}}} \|I_p - \mu_{\bar{\mathbf{s}}}\|_d \quad (3)$$

very common in clustering. In this case, the optimal value of parameter  $\mu$  may no longer correspond to a *mean*. For example, optimal  $\mu$  for  $L_1$  metric is a *median* and metric in (12) gives a *mode* [52, 13].

A seemingly different way to generalize Chan-Vese’s color clustering (2) is to treat both means and covariance matrices for the Gaussian models as variables. Then the likelihood term in (1) correspond to the standard *elliptic K-means* energy [55, 51, 20]. In this case optimized parameters  $\theta = \{\mu, \Sigma\}$  are not even in the same space as data points  $I_p$ . But, it is still possible to define the distance be-

<sup>1</sup>We use  $\stackrel{c}{=}$  and  $\stackrel{c}{\approx}$  for “up to additive constant” relations.

<sup>2</sup>Optimal bandwidth for accurate Parzen density estimation is near data resolution [60]. Such kernel width is too small for good clustering, Sec.4.1.

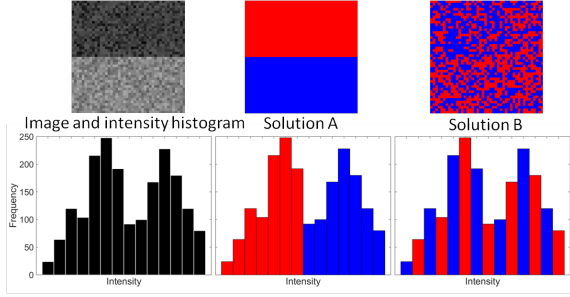


Figure 2: *Histograms in color spaces*. Entropy criterion (5) with histograms can not tell a difference between A and B: bin permutations do not change the histogram’s entropy.

tween point  $I_p$  and model  $\theta$  as distortion

$$\|I_p - \theta\|_d := -\log \mathcal{P}(I_p|\theta).$$

Elliptic K-means and distortion energy (3) are examples of a general class of *probabilistic K-means* methods [33] in Table 1B. This generalization of K-means corresponds to fitting arbitrary probability models, not necessarily Gaussian, extending energy (2) to

$$-\sum_{p \in \mathbf{S}} \log \mathcal{P}(I_p|\theta_s) - \sum_{p \in \bar{\mathbf{S}}} \log \mathcal{P}(I_p|\theta_{\bar{s}}) \quad (4)$$

where  $\theta_s$  are ML model parameters for each segment.

The name *probabilistic K-means* for energy (4) in the general clustering context was coined by [33]. They formulated (4) after representing distortion energy (3) as ML fitting of Gibbs models  $\frac{1}{Z_d} e^{-\|x - \mu\|_d}$  for integrable metrics. In computer vision, energy (4) with any probability models is known as the *log-likelihood term* for clustering colors, geometric or higher-level features  $\{I_p\}$ . Since data points correspond to pixels  $p$ , segmentation energies like (1) often combine probabilistic K-means (4) for features  $I_p$  with image domain regularization, e.g. Potts smoothness<sup>3</sup>. Typical models for (4) in vision are elliptic Gaussians [55, 51, 20], gamma/exponential [2], or other generative models [43]. As discussed, the corresponding parameters  $\theta$  or  $\mu$  are often different from the basic “mean”. Yet, *probabilistic K-means* is a good idiomatic name for general clustering energy (4).

Zhu-Yuille [64] and GrabCut [50] popularized fitting highly descriptive probability models (GMM or histograms) for color clustering in segmentation energies like (1). Assuming  $\mathcal{P}(\theta) \equiv \mathcal{P}(\cdot|\theta)$  is a continuous density of a sufficiently descriptive class (e.g. GMM), information theoretic analysis in [33] shows that probabilistic K-means energy (4) reduces to standard *entropy criterion* for clustering

$$\approx |\mathbf{S}| \cdot H(\mathbf{S}) + |\bar{\mathbf{S}}| \cdot H(\bar{\mathbf{S}}). \quad (5)$$

<sup>3</sup>Outside of vision, general *distortion* clustering (3) can use its probabilistic Gibbs representation in [33] to integrate Potts-like prior, see [3].

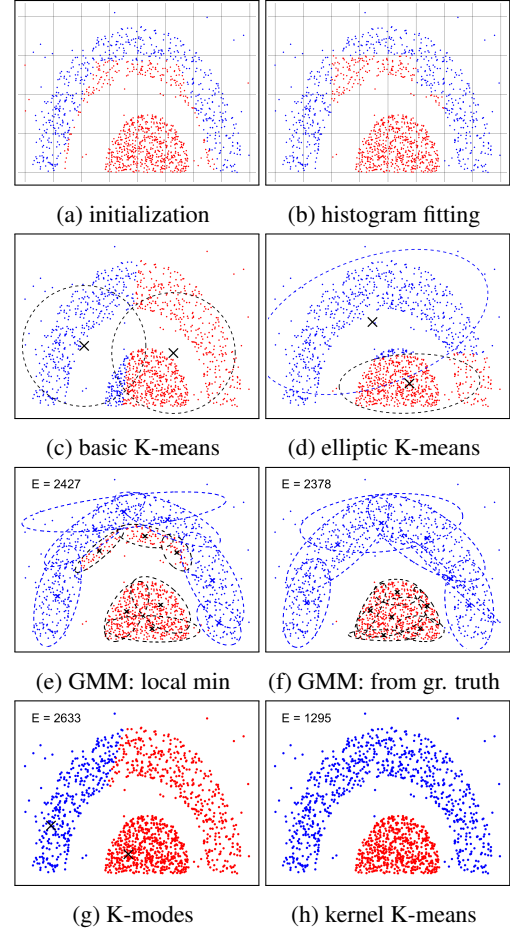


Figure 3: *Model fitting (4) vs kernel K-means (11)*. Histogram fitting always converges in one step assigning initially dominant bin label (a) to all points in the bin (b): energy (4,5) is minimal at any volume-balanced solution with one label inside each bin [33]. Basic and elliptic K-means (one mode GMM) under-fit the data (c,d). Six mode GMMs over-fit (e) similarly to histograms (b). GMMs have a local minimum issue; ground-truth initialization (f) yields lower energy (4,5). Proper kernel K-means formulation (10,11) with Gaussian kernel  $k$  in (h) outperforms its weaker point-wise version (17) with kernel distance  $\|\cdot\|_k$  and explicit estimation of  $\mu$  in (g), which can be seen as *K-modes* (18).

Indeed, for any function  $f(x)$  Monte-Carlo estimation gives  $\sum_{p \in \mathbf{S}} f(I_p) \approx |\mathbf{S}| \cdot \int f(x) d_s(x) dx \equiv |\mathbf{S}| \cdot \langle f, d_s \rangle$  where  $d_s$  is a “true” density for intensities in  $\mathbf{S}$  and  $\langle \cdot, \cdot \rangle$  is a dot product. If  $f = -\log \mathcal{P}(\theta_s)$  and  $d_s \approx \mathcal{P}(\theta_s)$  then (4) implies (5) for differential entropy  $H(\mathbf{S}) := H(\mathcal{P}(\theta_s))$ . For histograms  $\mathcal{P}_h(\mathbf{S}) \equiv \mathcal{P}_h(\cdot|\mathbf{S})$  entropy-based interpretation (5) of (4) is exact for discrete entropy  $H(\mathbf{S}) := -\sum_x \mathcal{P}_h(x|\mathbf{S}) \cdot \log \mathcal{P}_h(x|\mathbf{S}) \equiv -\langle \mathcal{P}_h(\mathbf{S}), \log \mathcal{P}_h(\mathbf{S}) \rangle$ .

Intuitively, minimization of the entropy criterion (5) fa-

vors clusters with tight or “peaked” distributions. This criterion is widely used in categorical clustering [41] or decision trees [12, 42] where the entropy evaluates histograms over “naturally” discrete features. Our paper demonstrates that the entropy criterion with either discrete histograms or continuous GMM densities has important limitations in the context of *continuous* color spaces.

In case of histograms, the key problem for color space clustering is illustrated in Fig.2. Once continuous color space is broken into bins, the notion of proximity between the colors in the nearby bins is lost. Since bin permutations do not change the histogram entropy, criterion (5) can not distinguish the quality of clusterings A and B in Fig.2; some permutation of bins can make B look very similar to A.

In case of continuous GMM densities, the problem of entropy criterion (5) is quite different. In general, continuous density estimators commonly use Gaussian kernels, which preserve the notion of continuity in the color space. Indeed, the (differential) entropy for any reasonable continuous density estimate will see a significant difference between the clusters in A and B, see Figure 2.

We observe that the main issue for entropy criterion (5) with GMM densities is related to optimization problems. In this case high-order energies (5) or (4) require joint optimization of discrete variables  $S_p$  and a large number of additional continuous parameters for optimum GMM density  $\mathcal{P}(\cdot|\theta_S)$ . That is, the use of complex parametric probability models leads to complex high-order *mixed* objective functions. Typical block coordinate descent methods [64, 50] iterating optimization of  $S$  and  $\theta$  are sensitive to local minima, see Figures 1 and 3(e). Better solutions like Figure 3(f) have lower energy, but they can not be easily found unless initialization is very good.

These problems of probabilistic K-means with histograms or GMM in color spaces may explain why descriptive model fitting is not common in the learning community for clustering high-dimensional continuous spaces. Instead of probabilistic K-means they often use a different extension of K-means, that is *kernel K-means* in Table 1C.

## 1.2. Towards Kernel K-means ( $k$ KM)

We propose *kernel K-means* energy to replace the standard likelihood term (4) in common regularization functionals for segmentation (1). In machine learning, kernel K-means ( $k$ KM) is a well established data clustering technique [57, 44, 26, 22, 17, 31], which can identify complex structures that are non-linearly separable in input space. In contrast to *probabilistic K-means* using complex models, see Tab.1, this approach maps the data into a higher-dimensional Hilbert space using a nonlinear mapping  $\phi$ . Then, the original non-linear problem often can be solved by simple linear separators in the new space.

Given a set of data points  $\{I_p | p \in \Omega\}$  kernel K-means

corresponds to the basic K-means in the embedding space. In case of two clusters (segments)  $S$  and  $\bar{S}$  this gives energy

$$E_k(S) := \sum_{p \in S} \|\phi(I_p) - \mu_S\|^2 + \sum_{p \in \bar{S}} \|\phi(I_p) - \mu_{\bar{S}}\|^2. \quad (6)$$

where  $\|\cdot\|$  denotes the Euclidean norm,  $\mu_S$  is the mean of segment  $S$  in the new space

$$\mu_S = \frac{\sum_{q \in S} \phi(I_q)}{|S|} \quad (7)$$

and  $|S|$  denotes the cardinality of segment  $S$ . Plugging  $\mu_S$  and  $\mu_{\bar{S}}$  into (6) gives equivalent formulations of this criterion using solely pairwise distances  $\|\phi(I_p) - \phi(I_q)\|$  or dot products  $\langle \phi(I_p), \phi(I_q) \rangle$  in the embedding space. Such equivalent pairwise energies are now discussed in detail.

It is a common practice to use *kernel function*  $k(x, y)$  directly defining the dot product

$$\langle \phi(x), \phi(y) \rangle := k(x, y) \quad (8)$$

and distance

$$\begin{aligned} \|\phi(x) - \phi(y)\|^2 &\equiv k(x, x) + k(y, y) - 2k(x, y) \\ &\equiv \|x - y\|_k^2. \end{aligned} \quad (9)$$

in the embedding space. *Mercer’s theorem* [45] states that any continuous *positive semi-definite* (p.s.d.) kernel  $k(x, y)$  corresponds to a dot product in some high-dimensional Hilbert space. The use of such kernels (a.k.a. *kernel trick*) helps to avoid explicit high-dimensional embedding  $\phi(x)$ .

For example, rewriting K-means energy (6) with pairwise distances  $\|\phi(I_p) - \phi(I_q)\|^2$  in the embedding space implies one of the equivalent  $k$ KM formulations in Tab.1C(i)

$$E_k(S) \equiv \frac{\sum_{pq \in S} \|I_p - I_q\|_k^2}{2|S|} + \frac{\sum_{pq \in \bar{S}} \|I_p - I_q\|_k^2}{2|\bar{S}|} \quad (10)$$

with isometric kernel distance  $\|\cdot\|_k^2$  as in (9). This *Hilbertian metric*<sup>4</sup> replaces Euclidean metric inside the basic K-means formula in the middle of Tab.1A. Plugging (9) into (10) yields another equivalent (up to a constant) energy formulation for  $k$ KM directly using kernel  $k$  without any explicit reference to embedding  $\phi(x)$

$$E_k(S) \stackrel{c}{=} - \frac{\sum_{pq \in S} k(I_p, I_q)}{|S|} - \frac{\sum_{pq \in \bar{S}} k(I_p, I_q)}{|\bar{S}|}. \quad (11)$$

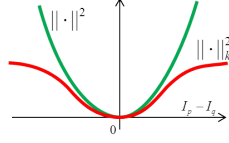
Kernel K-means energy (10) can explain the positive result for the standard Gaussian kernel  $k = \exp \frac{-(I_p - I_q)^2}{2\sigma^2}$  in Fig.3(h). Gaussian kernel distance (red plot below)

$$\|I_p - I_q\|_k^2 \propto 1 - k(I_p, I_q) = 1 - \exp \frac{-(I_p - I_q)^2}{2\sigma^2} \quad (12)$$

<sup>4</sup>Such metrics can be isometrically embedded into a Hilbert space [27].



is a “robust” version of Euclidean metric in basic K-means (green). Thus, Gaussian kernel K-means finds clusters with small local variances, Fig.3(h). In contrast, basic K-means (c) tries to find good clusters with small global variances, which is impossible for non-compact clusters.



Focusing on pairwise clustering criteria (10) and (11) raises a natural question: why should distortion measure  $\|x - y\|_k^2$  and similarity function  $k(x, y)$  be restricted to Hilbertian metrics and p.s.d. kernels? That is, why should one worry that there is some embedding  $\phi$  with an equivalent clustering energy (6)? There are two complimentary answers. On the one hand, the standard  $k$ KM algorithm [44, 26] directly corresponds to the basic iterative K-means procedure for (6) even though it avoids explicit embedding  $\phi$  due to pairwise formulation with kernels, see Sec.2. Thus,  $k$ KM algorithm convergence is not guaranteed for improper metrics or kernels. On the other hand, pairwise energies (10) and (11) for proper  $k$  are general enough. The next subsection shows that generalizations to arbitrary distortion and similarity measures are not essential as there exist p.s.d. kernels with equivalent (up to constant)  $k$ KM energies.

**Average distortion (AD) or association (AA):** Equivalent formulations for energy  $E_k$  in (10) and (11) suggest natural extensions of kernel K-means. For example, dropping p.s.d. assumption for kernels one can replace  $k$  in (11) with arbitrary pairwise similarities or affinities  $A = [A_{pq}]$  defining standard *average association* (AA) energy

$$E_A(\mathbf{S}) := -\frac{\sum_{pq \in \mathbf{S}} A_{pq}}{|\mathbf{S}|} - \frac{\sum_{pq \in \bar{\mathbf{S}}} A_{pq}}{|\bar{\mathbf{S}}|}. \quad (13)$$

Kernel K-means energy (11) is a special case of (13) for  $A_{pq} = k(I_p, I_q)$ . Similarly, Hilbertian metric  $\|\cdot\|_k^2$  in (10) can be replaced by arbitrary zero-diagonal distortion matrix  $D = [D_{pq}]$  generating *average distortion* (AD) energy

$$E_D(\mathbf{S}) := \frac{\sum_{pq \in \mathbf{S}} D_{pq}}{2|\mathbf{S}|} + \frac{\sum_{pq \in \bar{\mathbf{S}}} D_{pq}}{2|\bar{\mathbf{S}}|}. \quad (14)$$

Kernel K-means energy (10) is a special case of (14) for  $D_{pq} = \|I_p - I_q\|_k^2$ . Below we discuss equivalence relationships between  $k$ KM, AD, and AA energies. Figure 4 illustrates these relations in a more general weighted case.

Despite dropping metric and proper kernel assumptions, average distortion (14) and average association (13) clustering criteria can be reduced to  $k$ KM for arbitrary associations  $A$  and any zero-diagonal distortions  $D$ . For example, it is easy to check that any matrix  $A$  in (13) can be equivalently replaced by “kernel matrix”

$$k := \frac{A + A^T}{2} + \lambda \cdot I \quad (15)$$

without changing energy (13), up to a constant. For sufficiently large scalar  $\lambda$  matrix  $k$  is positive definite yielding proper discrete kernel  $k_{pq} \equiv k(I_p, I_q) : \chi \times \chi \rightarrow \mathcal{R}$  for finite set  $\chi = \{I_p | p \in \Omega\}$ . Eigen decomposition for kernel matrix  $k = V^T \Lambda V$  allows an explicit finite-dimensional Euclidean embedding<sup>5</sup> satisfying isometry (9)

$$\phi(I_p) = \sqrt{\Lambda} V_p \in \mathcal{R}^{|\Omega|}$$

where  $V_p$  is a column (eigen vector) in matrix  $V$  and  $\Lambda$  is a diagonal matrix of eigen values. Indeed, as in (8)

$$\langle \phi(I_p), \phi(I_q) \rangle = (\sqrt{\Lambda} V_p)^T (\sqrt{\Lambda} V_q) = k_{pq}.$$

Non-negativity of eigen values for  $k$  is important for decomposition  $\Lambda = \sqrt{\Lambda} \cdot \sqrt{\Lambda}$ . K-means for the embedded points  $\phi(I_p)$  corresponds to average association energy (11) for matrix (15), which is equivalent to (13) up to a constant.

Since average distortion energy (14) for arbitrary  $D$  is equivalent to average association for  $A = -\frac{D}{2}$ , it can also be converted to  $k$ KM as above. Using the corresponding kernel (15) and (9) it is easy to derive Hilbertian distortion (metric) equivalent to original distortions  $D$

$$\|I_p - I_q\|_k^2 := \frac{D + D^T}{2} + 2\lambda(ee^T - I) \quad (16)$$

where  $ee^T$  is a matrix where all entries are 1.

The above reduction of AD and AA to  $k$ KM summarizes the technical results in Roth et al. [49]. Dhillon et al. [22, 21] also reduce *normalized cut* [54] to a weighted version of  $k$ KM. In Section 3 we present a simpler proof showing that normalized cuts is a special case of weighted AA directly from the definition in [54]. Our Figure 4 outlines equivalence relations between  $k$ KM, AD and AA in the general case of weighted data points. These reductions to  $k$ KM allow to apply our bound and *pseudo-bound* optimization approach (Sec.2) to arbitrary weighted AD and AA criteria including normalized cuts. In particular, they can be combined with standard geometric and MRF-based regularizers and constraints. For simplicity, most of the paper is presented in the context of non-weighted kernel K-means energies  $E_k$  defined in (6-11).

**Pairwise vs. pointwise distortions:** Equivalence of  $k$ KM to pairwise distortion criteria (14) helps to juxtapose *kernel K-means* with *probabilistic K-means* (Sec.1.1) from a point of view complimentary to Table 1. Both methods generalize the basic K-means (2) by replacing Euclidean metric with a more general distortion measure  $\|\cdot\|_d$ . But,  $k$ KM uses “pairwise” formulation (10) where  $\|\cdot\|_d = \|\cdot\|_k^2$  measures distortion between pairs of points, while  $p$ KM

<sup>5</sup>Mercer’s theorem for continuous p.d. kernels  $k(x, y)$  uses a similar eigen decomposition giving infinite-dimensional Hilbert embedding  $\phi(x)$ . Our discrete kernel embedding  $\phi(I_p)$  has finite dimension  $|\Omega|$ , which is still much higher than the dimension of points  $I_p$ , e.g.  $\mathcal{R}^3$  for colors.

uses “pointwise” formulation (3) where  $\|\cdot\|_d$  measures distortion between a point and a model. Even though these formulations are equivalent for Euclidean distortion (*i.e.* basic K-means), they are very different in general, see Figure 5.

For example,  $k$ KM energy (10) for data points  $\{I_p | p \in \Omega\}$  is defined by a finite set of pairwise distortions represented by matrix  $D_{pq} = \|I_p - I_q\|_d$  in (14). In contrast, pKM energy (3) uses pointwise distortion  $\|I_p - \theta\|$  where the second argument is typically a continuous model parameter. While parameter  $\theta$  is often in the same space as data points, it does not have to be in general. For instance, elliptic K-means uses Gaussians with  $\theta = (\mu, \Sigma)$ . Thus, general pointwise distortions for pKM correspond to *likelihoods*  $\|I_p - \theta\|_d = -\ln \mathcal{P}(I_p | \theta)$  in (4) where points  $I_p$  and model parameters  $\theta$  could be in different spaces.

In summary, pKM methods are essentially ML model-fitting techniques jointly optimizing clustering  $S$  and explicit parameters  $\theta$  using pointwise distortions (3) or likelihoods (4) representing distances between data points and models. In contrast,  $k$ KM methods use pairwise distortions (10) or (14) minimizing distances between pairs of points within each cluster. Yet,  $k$ KM is equivalent to basic K-means (6) implicitly optimizing cluster means  $\mu$  in some isometric high-dimensional embedding space.

**Weak kernel K-means:** For Hilbertian distortions  $\|\cdot\|_d = \|\cdot\|_k^2$  with p.s.d. kernels we can show that pairwise  $k$ KM approach (10) is “stronger” than a pointwise pKM approach (3) using the same metric. In this case pKM can be called *weak kernel K-means*, see Figure 5. Equivalent  $k$ KM formulation (6) guarantees more complex decision boundaries, see Fig.3(h), compared to pKM energy (3)

$$\begin{aligned} & \sum_{p \in S} \|I_p - \mu_S\|_k^2 + \sum_{p \in \bar{S}} \|I_p - \mu_{\bar{S}}\|_k^2 \\ &= \sum_{p \in S} \|\phi(I_p) - \phi(\mu_S)\|^2 + \sum_{p \in \bar{S}} \|\phi(I_p) - \phi(\mu_{\bar{S}})\|^2 \end{aligned} \quad (17)$$

with isometric kernel distance  $\|\cdot\|_k$  and explicit  $\mu$  in the original space, Fig.3(g). Indeed, any  $\mu$  in the original space corresponds to some search point  $\phi(\mu)$  in the high-dimensional embedding space, while the opposite is false. Thus, optimization of (10) and (6) has larger search space than (17). It is also easy to check that energy (17) is an upper bound for (10) at any  $S$ . For this reason we refer to distortion energy (17) with kernel distance  $\|\cdot\|_k$  and explicit  $\mu$  in the original space as *weak kernel K-means*. Pointwise energy (17) is an example of pKM (3), while pairwise energy (10) with the same kernel metric is the regular  $k$ KM. Note that weak kernel K-means (17) for Gaussian kernel corresponds to  $K$ -modes, see Fig.3(g) and Sec.1.3.

Figure 5 illustrates relations between kernel K-means (10) and probabilistic K-means (3,4). It includes a few examples discussed earlier and more examples from Sec.1.3.

### 1.3. Previous kernel methods in segmentation

One of our goals is to combine kernel K-means clustering in the feature (color) space with standard constraints and regularization techniques (geometric or MRF) in the spacial domain. Figure 5 and Table 2 illustrate the general context of this work helping to relate our kernel approach to prior optimization-based segmentation and clustering methods.

**Pairwise clustering, normalized cuts, etc.:** Section 1.2 has already discussed strong relations between  $k$ KM and general *pairwise clustering* criteria such as *average distortion* (14), *average association* (13), and normalized cuts. Figure 4 summarizes these relations for the general case of weighted points. Relations of kernel-based clustering to many common binary segmentation energies with a single ratio term [19, 32, 59, 36, 28] are not clear and they are left outside the scope of this work.

There are several existing methods for approximate optimization of NP-hard pairwise clustering energies discussed in this paper. Shi, Malik, and Yu [54, 62] popularized *spectral relaxation* methods in the context of normalized cuts. Such methods also apply to AA and other problems [54]. E.g., similarly to [62] one can rewrite AA energy (13) as

$$E_A(S) = -\text{tr}(Z^T A Z) \quad \text{for } Z := \begin{bmatrix} \mathbf{S} & \bar{\mathbf{S}} \\ \sqrt{|\mathbf{S}|} & \sqrt{|\bar{\mathbf{S}}|} \end{bmatrix}$$

where  $Z$  is a  $\Omega \times 2$  matrix of normalized indicator vectors  $\mathbf{S}$  and  $\bar{\mathbf{S}}$ . Orthogonality  $\mathbf{S}^T \bar{\mathbf{S}} = 0$  implies  $Z^T Z = I_2$  where  $I_2$  is an identity matrix of size  $2 \times 2$ . Minimization of the *trace* energy above with relaxed  $Z$  constrained to a unit sphere  $Z^T Z = I_2$  is a simple representative example of *spectral relaxation* in the context of AA. This relaxed trace optimization is a generalization of *Rayleigh quotient* problem that has an exact closed form solution in terms of two largest eigen vectors for matrix  $A$ . This approach extends to general multi-label weighted AA and related graph clustering problems, *e.g.* normalized cuts and ratio cuts [54, 62]. The main computational difficulties for spectral methods are explicit eigen decomposition for huge matrices and integrality gap due to heuristics for extracting integer solutions for the original combinatorial problem.

Buhmann et al. [29, 49] address the general AD and AA energies via mean field approximation and *deterministic annealing*. It can be seen as a *fuzzy version*<sup>6</sup> of kernel K-means algorithm. In the context of normalized cuts Dhillon et al. [22, 21] use spectral relaxation to initialize  $k$ KM algorithm.

One of our contributions is a formulation of the standard iterative  $k$ KM algorithm as a bound optimizer for the general pairwise clustering energies. In particular, this allows pseudo-bound optimization [56]. Moreover, our bound-based framework can easily combine pairwise clustering criteria with standard MRF and geometric regularization.

<sup>6</sup>Fuzzy version of K-means in Duda et al. [23] generalizes to  $k$ KM.

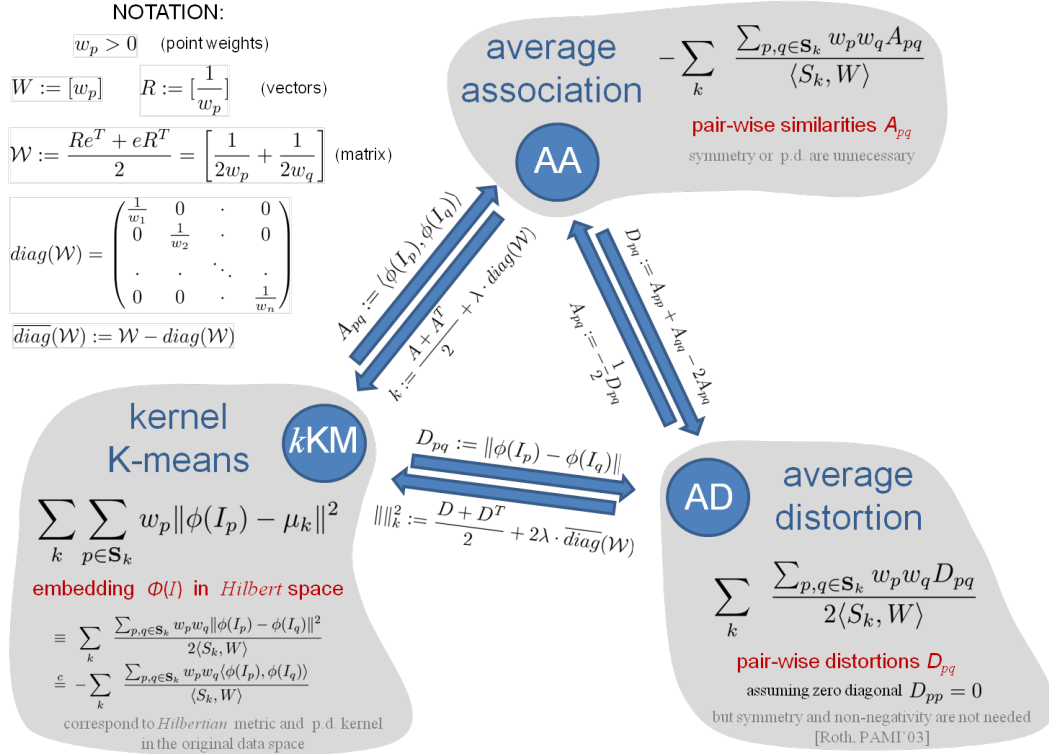


Figure 4: Equivalence of clustering methods: *kernel K-means* (*kKM*), *average distortion* (*AD*), *average association* (*AA*). We present the general case of weighted points. Typically, *kKM* is associated with *positive-definite* (p.d.) or *conditionally positive-definite* (c.p.d.) kernels [53] and Hilbertian distortions [27]. The above formulations of *AA* and *AD* make no assumptions for association matrix *A* and distortions *D* except for zero diagonal in *D*. Then, equivalence of *AD* and *AA* objectives (up to a constant) is straightforward. Roth et al. [49] reduce non-weighted case of *AD* to *kKM*. For arbitrary *D* they derive Hilbertian distortion  $\|\cdot\|_k^2$  with an equivalent *AD* energy (up to a constant) and explicitly construct the corresponding embedding  $\phi$ . We show Hilbertian metric  $\|\cdot\|_k^2$  for the general weighted case of *AD*, see *AD*→*kKM* above. Dhillon et al. [22, 21] prove that *normalized cuts* is a special case of weighted *kKM* and construct the corresponding p.d. kernel. Sec.3 shows a simpler reduction of *normalized cuts* to weighted *AA*. Similarly to [49], an equivalent p.d. kernel could be constructed for any association matrix *A*, see *AA*→*kKM* above and Sec.3. Note that the formulas for *A*-equivalent p.d. kernel and *D*-equivalent Hilbertian metric require some sufficiently large scalar  $\lambda$ . Roth et al. [49] relate proper  $\lambda$  to the smallest eigen value of  $A = -\frac{D}{2}$ . Our weighted formulation requires the eigen value of  $\text{diag}(\mathcal{W})^{-\frac{1}{2}} \cdot A \cdot \text{diag}(\mathcal{W})^{-\frac{1}{2}}$ . Applying *pseudo-bound* optimization [56] to *kKM* can bypass an expensive computation of eigen values. Indeed, term  $\lambda \cdot \text{diag}(\mathcal{W})$  generates a monotone *perturbation* for our *kKM* bound. The corresponding pseudo-bounds for all  $\lambda$  can be efficiently explored by parametric max-flow in [56]. For the algorithm to work it is enough that some (unknown)  $\lambda$  gives a proper bound.

In the context of image segmentation pairwise clustering is typically applied to RGBXY space using spectral relaxation, see Tab.2. Unification of the color space and the image domain is a standard way to enforce segmentation boundary smoothness in this framework. Common MRF or geometric energies typically combine unary data (color) and arbitrary regularization terms in a linear fashion as in (1). In contrast, it is not easy to integrate specific constraints on geometry, shape, or sparsity into spectral methods for pairwise clustering. For example, to combine *kKM* with Potts regularization [37] normalizes the corresponding pairwise constraints by cluster sizes. This alters the Potts model to fit

the problem to a standard trace-based formulation, which is analogous to RGBXY clustering in the context of segmentation. In contrast, our bound formulation allows to combine *kKM* clustering term with the exact Potts and other priors.

Adding non-homogeneous linear constraints into spectral relaxation techniques also requires additional approximations [63] or some model modifications [61]. Exact optimization for the relaxed quadratic ratios (including *normalized cuts*) with arbitrary linear equality constraints is possible by solving a sequence of spectral problems [24].

We propose a proper bound (surrogate function) for *kKM* that allows pseudo-bound optimization [56]. Without com-

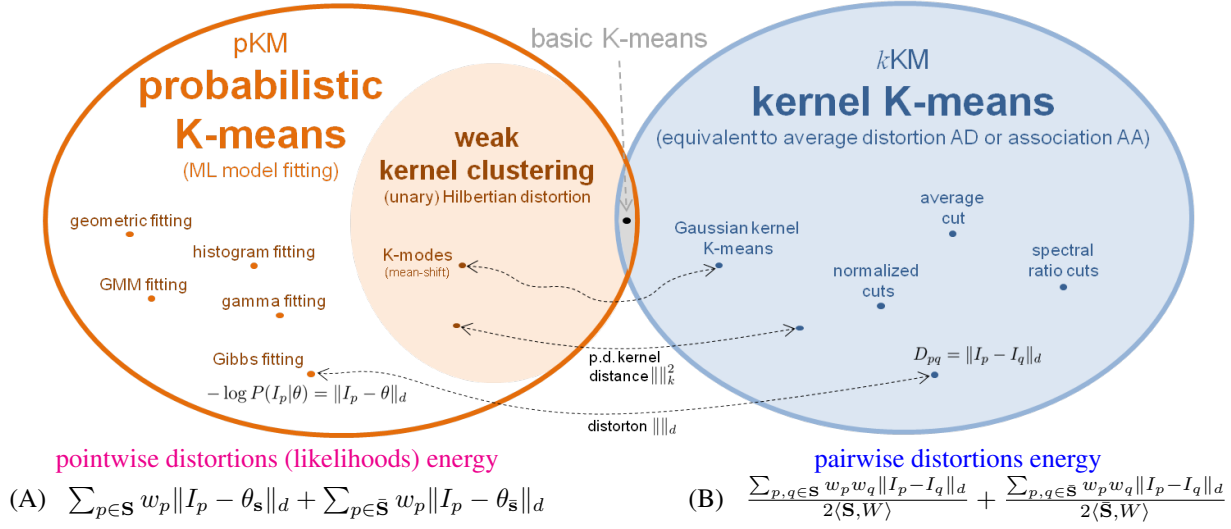


Figure 5: Clustering with (A) pointwise and (B) pairwise distortion energies generalizing (3) and (14) for points with weights  $W = \{w_p\}$ . Pointwise distortion relates a data point and a model as log-likelihood function  $\|I_p - \theta\|_d = -\ln \mathcal{P}(I_p|\theta)$ . Pairwise distortion is defined by matrix  $D_{pq} = \|I_p - I_q\|_d$ . Weighted AD or AA for arbitrary metrics are equivalent to weighted  $k$ KM, see Figure 4. As shown in [49, 22] *average cut*, *normalized cut* [54], and *spectral ratio cut* [47] are examples of (weighted)  $k$ KM. Our (pseudo-) bound optimization for  $k$ KM extends to any weighted pairwise distortion energy (B).

| standard model fitting approaches [64, 14, 50, 52]   | standard kernel approaches [54, 18] |
|--|-------------------------------------|
| + RGB clustering (model fitting)<br>+ XY regularization (e.g. MRF)<br>+ sparsity (e.g. label cost) | RGBXY clustering (e.g. spectral)    |
| our approach: kernel K-means with regularization   |                                     |
| + RGB kernel clustering<br>+ XY regularization<br>+ sparsity (e.g. label cost)                     | (bound optimization)                |

Table 2: Standard image segmentation methods and our approach. RGB is the space of observed features (colors)  $I_p$  at each pixel  $p$  in XY - the spacial domain or image grid. Standard regularization methods for XY integrate geometric priors (segmentation boundary length, curvature, shape prior). Clustering in unified RGBXY space complicates the use of specific geometric priors. Joining regularization in XY with kernel approach to RGB allows to combine the benefits of well-known geometric or MRF methods and powerful kernel clustering techniques extendable to high-dimensional features  $I_p$ .

putting expensive eigen decomposition, the method applies to general pairwise clustering energies AD and AA. Such energies for RGB (feature) space can be combined with any standard (e.g. MRF) or geometric regularization in XY domain and *label cost* sparsity terms [20].

**K-modes and mean-shift:** Weak kernel K-means using unary formulation (3) with kernel distance  $\|\cdot\|_k$  and explicit optimization of  $\mu$  in the original data space is closely related to *K-modes* approach to clustering continuous [13] or

discrete [30, 15] data. For example, for Gaussian kernel distance  $\|\cdot\|_k$  energy (3) becomes

$$-\sum_{p \in \mathbf{S}} e^{-\frac{\|I_p - \mu_{\mathbf{s}}\|^2}{2\sigma^2}} - \sum_{p \in \bar{\mathbf{S}}} e^{-\frac{\|I_p - \mu_{\bar{\mathbf{s}}}\|^2}{2\sigma^2}}$$

which can be rewritten using Parzen densities as

$$= -\mathcal{P}_k(\mu_{\mathbf{s}}|\mathbf{S}) - \mathcal{P}_k(\mu_{\bar{\mathbf{s}}}|\bar{\mathbf{S}}). \quad (18)$$

Clearly, optimal  $\mu_{\mathbf{s}}$  and  $\mu_{\bar{\mathbf{s}}}$  are Parzen density modes in each



segment. K-modes objective (18) can be seen as an energy-based formulation of mean-shift clustering [16, 18] with a fixed number of clusters. Formal objective allows to combine color clustering via (18) with geometric regularization in the image domain [52]. If needed, the number of clusters (modes) can be regularized by adding *label cost* [20]. In contrast, mean-shift segmentation [18] clusters RGBXY space combining color and spatial information. The number of clusters is indirectly controlled by the bandwidth. Appendix C extends our K-modes/mean-shift discussion.

**Parzen-based entropy clustering:** non-parametric kernel (Parzen) densities can be used to approximate entropy criterion (5), e.g. [34, 35], even though their *mutual information* narrative may seem different. This approximation for color clustering can be combined with geometric spacial regularization. The corresponding complex optimization problem is addressed by gradient descent via level sets [35], which is slow and prone to local minima, or by computationally expensive quadratic bounds [34]. It would be interesting to compare with our kernel K-means method, but their code or results on public data-sets are not available.

#### 1.4. Summary of contributions

We propose kernel K-means as feature/color clustering criteria in combination with standard regularizers in the image domain. This combination is possible due to our bound formulation for  $k$ KM allowing to incorporate standard regularization algorithms such as max-flow. Our general framework applies to multi-label segmentation (supervised or non-supervised). Our approach is a new extension of K-means for color-based segmentation [14] different from probabilistic K-means [64, 50]. As special cases, our  $k$ KM color clustering term includes *average distortion*, *average association*, *normalized cuts* and other pairwise clustering criteria (Sec.1.3) previously used for segmentation in a different setting [54, 29].

Our bound formulation for  $k$ KM also allows *pseudo-bound* optimization [56]. Besides regularized segmentation framework above, this approach also applies to standard pairwise clustering, including normalized cuts. Pseudo-bound approach can improve standard iterative  $k$ KM algorithms and may compete with spectral relaxation methods for general (weighted) AD and AA problems while avoiding expensive eigen decompositions. More experiments should fully evaluate the potential of this optimization approach to general graph clustering energies.

Our  $k$ KM approach to color clustering has several advantages over standard probabilistic K-means methods [64, 50] based on histograms or GMM (Sec.1.1). In contrast to histograms, kernels preserve color space continuity without breaking it into unrelated bins, see Figure 2. Unlike GMM, our use of non-parametric kernel densities avoids mixed optimization over a large number of additional model-fitting

variables. This reduces sensitivity to local minima, as illustrated in Figure 3(e,h).

For high-dimensional applications, kernel methods are a prevalent choice in the learning community as EM becomes intractable for high dimensions. Thus, our segmentation method extends to higher dimensional feature spaces.

Our approach allows arbitrary kernels or distortion measures. As a proof-of-the-concept, this paper focuses on the most standard Gaussian and 0-1 (KNN) kernels and discusses bandwidth selection strategies (adaptive and non-adaptive). We analyze the extreme bandwidth cases (Sec.4). It is known that for wide kernels (approaching data range)  $k$ KM converges to basic K-means, which has bias to equal size clusters [33, 8]. It has been observed empirically that small-width kernels (approaching data resolution) show bias to compact dense clusters [54]. We provide a theoretical explanation for this bias by connecting  $k$ KM energy for small bandwidth with the *Gini criterion* for clustering (36). We analytically prove the bias to compact dense clusters for the continuous case of Gini, see Theorem 1, extending the previous result for histograms by Breiman [12].

We also propose a class of adaptive bandwidth strategies. We use Nash theorem to obtain such strategies from density transformations (Nash embedding). That is, adaptive kernels work as “density equalization” techniques. Our experiments show state-of-the-art-performance even with the most straightforward Gaussian kernels. Other kernels, weighted points, learning techniques, and applications to higher-dimensional features are left to future work.

$k$ KM methods could be expensive for large image analysis problems. General kernels (e.g. Gaussian) imply quadratic complexity of each iteration due to high connectivity of the graph. We propose an efficient parallel implementation for our bound optimization framework that applies to general (e.g. adaptive) kernels.

## 2. Bound Optimization

In general, bound optimizers are iterative algorithms that optimize *auxiliary functions* (upper bounds) for a given energy  $E(\mathbf{S})$  assuming that these auxiliary functions are more tractable than the original difficult optimization problem [38, 56].  $A_t(\mathbf{S})$  is an auxiliary function of  $E(\mathbf{S})$  at current solution  $\mathbf{S}_t$  ( $t$  is the iteration number) if:

$$E(\mathbf{S}) \leq A_t(\mathbf{S}) \quad \forall \mathbf{S} \quad (19a)$$

$$E(\mathbf{S}_t) = A_t(\mathbf{S}_t) \quad (19b)$$

To minimize  $E(\mathbf{S})$ , we iteratively minimize an auxiliary function at each iteration  $t$ :  $\mathbf{S}_{t+1} = \arg \min_{\mathbf{S}} A_t(\mathbf{S})$ . It is easy to show that such an iterative procedure decreases original function  $E(\mathbf{S})$  at each step:

$$E(\mathbf{S}_{t+1}) \leq A_t(\mathbf{S}_{t+1}) \leq A_t(\mathbf{S}_t) = E(\mathbf{S}_t).$$

For example, iterative optimization in standard GrabCut algorithm [50] was shown to be an optimizer of a cross-entropy bound [56], see Table 1C(iii).

**Proposition 1.** *The following is an auxiliary function for the  $k$ KM formulation in (11)*

$$\begin{aligned} E_k(\mathbf{S}) &= -\frac{\sum_{pq \in \mathbf{S}} k_{pq}}{|\mathbf{S}|} - \frac{\sum_{pq \in \bar{\mathbf{S}}} k_{pq}}{|\bar{\mathbf{S}}|} \leq A_t(\mathbf{S}) \quad \text{where} \\ A_t(\mathbf{S}) &= -2 \sum_{p \in \mathbf{S}} \frac{\sum_{q \in \mathbf{S}_t} k_{pq}}{|\mathbf{S}_t|} - 2 \sum_{p \in \bar{\mathbf{S}}} \frac{\sum_{q \in \bar{\mathbf{S}}_t} k_{pq}}{|\bar{\mathbf{S}}_t|} \\ &\quad + |\mathbf{S}| \frac{\sum_{pq \in \mathbf{S}_t} k_{pq}}{|\mathbf{S}_t|^2} + |\bar{\mathbf{S}}| \frac{\sum_{pq \in \bar{\mathbf{S}}_t} k_{pq}}{|\bar{\mathbf{S}}_t|^2}. \end{aligned} \quad (20)$$

*Proof.* See Appendix A.  $\square$

**Proposition 2.** *The kernel  $K$ -means algorithm is a bound-optimization technique. In fact, the following standard updates [21] optimize  $A_t(\mathbf{S})$  at each iteration  $t$ :*

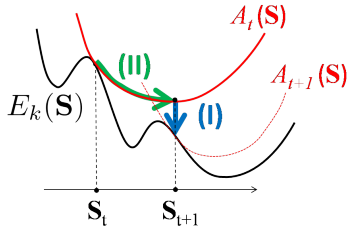
(I): *For each point  $p$  and cluster  $S^i$ , compute the distance between  $p$  and the mean of  $S^i$  in feature space:*

$$\text{dist}(p, S^i) = \left\| \phi(I_p) - \frac{\sum_{q \in S^i} \phi(I_q)}{|S^i|} \right\|^2 \quad (21)$$

(II): *Assign each point to the closest cluster:*

$$p \in S^j \text{ if } j = \arg \min_i \text{dist}(p, S^i) \quad (22)$$

In appendix A we clarify how these two standard steps in each iteration of the  $k$ KM algorithm yield a bound optimizer (see illustration below). In fact, step II (point re-assignment) globally optimizes auxiliary function  $A_t(\mathbf{S})$ . Step I (distance re-computation) gives new auxiliary function  $A_{t+1}(\mathbf{S})$  at  $S_{t+1}$ . It is not clear how to combine steps (I) and (II) with standard image-domain regularization. For example, to combine  $k$ KM with the Potts model [37]



normalizes the corresponding pairwise constraints by cluster sizes. This alters the Potts model to a form that accommodates trace-based formulation. In contrast, our bound-optimization interpretation allows to combine  $k$ KM or equivalent pairwise clustering energies AD and AA with any standard (e.g. MRF) or geometric regularization in XY domain. Furthermore, in Sec.3 we will generalize the kernel-based auxiliary function in (20) to arbitrary affinities  $A_{pq}$  and propose a pseudo-bound optimization technique that can handle the most general class of pairwise clustering energies, including various popular criteria

such as normalized cuts. Unlike spectral methods, our pseudo-bound framework removes the need for expensive eigen-value computations.

**Image segmentation functional:** We propose to minimize the following high-order functional for image segmentation, which combines image-plane regularization with the pairwise clustering energy  $E_k(\mathbf{S})$  in (11):

$$E(\mathbf{S}) = E_k(\mathbf{S}) + \beta R(\mathbf{S}) \quad (23)$$

where  $\beta$  is a (positive) scalar and  $R(\mathbf{S})$  is any functional with an efficient optimizer, e.g. a submodular boundary regularization term optimizable by max-flow methods

$$R(\mathbf{S}) = \sum_{\{p,q\} \in \mathcal{N}} l_{pq} [s_p \neq s_q] \quad (24)$$

where  $[\cdot]$  are Iverson brackets and  $\mathcal{N}$  is the set of neighboring pixels. Pairwise weights  $l_{pq}$  are evaluated by the spatial distance and color contrast between pixels  $p$  and  $q$  as in [9].

From proposition 1, it follows that  $A_t(\mathbf{S}) + \beta R(\mathbf{S})$  is an auxiliary function of high-order segmentation functional  $E(\mathbf{S})$  in (23). Furthermore, this auxiliary function is a combination of unary (modular) term  $A_t(\mathbf{S})$  and a sub-modular term  $R(\mathbf{S})$ . Therefore, at each iteration of step II for our bound optimization algorithm, the global optimum of the bound can be obtained efficiently in low-order polynomial time by solving an equivalent max-flow problem [10]. Step I of our algorithm requires evaluation of the auxiliary function (20), which has quadratic complexity ( $O(N^2)$ ). Section 5 discusses efficient implementation of step I.

### 3. Generalization to weighted AA

For completeness, this section considers  $K$  label case for a generalization of the formulation in (13) to weighted average association for given  $W := \{w_p | p \in \Omega\}$

$$E_A^W = - \sum_k \frac{\sum_{p,q \in S^k} w_p w_q A_{pq}}{\langle S^k, W \rangle}. \quad (25)$$

The study of this energy is motivated by the works of Roth et al. [49] and Dhillon et al. [22]. We show how to convert general energy (25) to weighted  $k$ KM naturally extending the arguments for reducing non-weighted AA to  $k$ KM in [49]. Moreover, we provide a bound for arbitrary affinities  $A$  enabling pseudo-bound optimization [56]. One of the motivations for studying (25) is the fact that *normalized cuts* [54, 62] is a special case of weighted AA, as shown later in this section. While our derivation is inspired by the well-known reduction of normalized cuts to weighted  $k$ KM in [22, 21], we propose an equivalence argument much simpler than their connection via trace optimization.

First, we reduce weighted AA to weighted  $k$ KM. This is trivial if  $A$  is a psd. Indeed, it is easy to check that (25) is

equivalent to a weighted version of  $k$ KM (see Fig. 4)

$$\sum_k \sum_{p \in S^k} w_p \|\phi(I_p) - \mu_{S^k}\|^2 \quad (26)$$

where

$$\mu_{S^k} := \frac{\sum_{p \in S^k} w_p \phi(I_p)}{\langle S^k, W \rangle} \quad (27)$$

is a weighted mean of segment  $S^k$  in the embedding space. Indeed, plugging (27) into (26) gives (25) up to a constant.

For the reduction of energy (25) to weighted  $k$ KM when  $A$  is not psd it is sufficient to design a psd kernel with an equivalent weighted AA energy. Such kernel can be build using the following basic algebraic Proposition.

**Proposition 3.** (e.g. Roth et al. [49]) *For any symmetric matrix  $M$  define*

$$\tilde{M} := M + \lambda I$$

where  $I$  is an identity matrix. Then, matrix  $\tilde{M}$  is positive semi-definite (psd) for any scalar  $\lambda \geq -\lambda_0(M)$  where  $\lambda_0$  is the smallest eigen value of its argument.

Indeed, as suggested in our Fig.4, it is easy to check that any matrix  $A$  can be equivalently replaced by the following matrix  $k$  without changing energy (25) (up to a constant)

$$k := \frac{A + A^T}{2} + \lambda \cdot \text{diag}(\mathcal{W}) \quad (28)$$

where  $\text{diag}(\mathcal{W})$  is a diagonal matrix with diagonal elements  $\frac{1}{w_p}$  for  $p \in \Omega$ . If (28) is rewritten in the following form

$$k = \text{diag}(\mathcal{W})^{\frac{1}{2}} (A^{\mathcal{W}} + \lambda \cdot I) \text{diag}(\mathcal{W})^{\frac{1}{2}} \quad \text{for} \quad A^{\mathcal{W}} := \text{diag}(\mathcal{W})^{-\frac{1}{2}} \left( \frac{A + A^T}{2} \right) \text{diag}(\mathcal{W})^{-\frac{1}{2}} \quad (29)$$

then Proposition 3 easily implies that (28) is psd for any scalar  $\lambda \geq -\lambda_0(A^{\mathcal{W}})$ . Note that [49] use Prop.3 for building psd kernels in the simpler case of (25) when  $\mathcal{W} = I$ .

A weighted version of the average distortion energy (14) is equivalent to (25) for  $A = -\frac{D}{2}$ . Therefore, weighted AD can also be converted to  $k$ KM as above, see Fig. 4.

Reduction of weighted AA or AD to  $k$ KM using equivalent psd kernels in (28) allows to write down an explicit bound for these energies. However, the use of (28) requires proper  $\lambda$  based on eigen values. Section 3.1 shows a *pseudo-bound* approach as in [56] that efficiently optimizes our energies without an expensive eigen decomposition.

**Normalized cuts is an example of weighed AA:** Dhillion et al. [22, 21] established the link between normalized cuts and weighted  $k$ KM showing that both problems can be transformed into a trace optimization for specific choices of weights and affinities. However, their proof is

quite lengthy and algebraically involved. Below we demonstrate these links in a much simpler way using a trivial conversion of normalized cuts energy to weighted AA objective directly based on their definitions in [54, 62] and (25).

Consider the following affinity matrix

$$\tilde{A} = \text{diag}(\mathcal{W}) \cdot A \cdot \text{diag}(\mathcal{W}) \quad (30)$$

where diagonal elements  $\frac{1}{w_p}$  for matrix  $\text{diag}(\mathcal{W})$  are defined by weights

$$w_p = \sum_{q \in \Omega} A_{pq}.$$

Indeed, plugging these  $\tilde{A}$  and  $w$  into weighted AA energy (25) immediately gives the well-known normalized cuts cost function [54, 62] with affinity matrix  $A$

$$-\sum_k \frac{\sum_{p,q \in S^k} A_{pq}}{\sum_{p \in S^k, q \in \Omega} A_{pq}} = -\sum_k \frac{\text{assoc}(S^k, S^k)}{\text{assoc}(S^k, \Omega)}. \quad (31)$$

In case of Gaussian kernel affinities  $A$  as used in [54] both  $A$  and  $\tilde{A}$  are positive definite matrices, which proves that (25) and, consequently, (31) are examples of  $k$ KM energy (26). In a more general case, the connection to  $k$ KM follows from the equivalent psd kernel (28)<sup>7</sup> discussed earlier.

### 3.1. Pseudo-bound optimization (no eigen values)

In this section, we propose a *pseudo-bound* optimization technique for energy (25). Pseudo bounds [56] can be used for avoiding weak local minima and to alleviate the need for computing eigen decompositions for large matrices. For simplicity, we focus on the binary case  $K = 2$ , but we will discuss extensions to multi-label optimization at the end.

Let us recall the following definition introduced in [56].

**Definition 1. (Pseudo-bound [56])** *Given an energy  $E(\mathbf{S})$ , current solution  $\mathbf{S}_t$  and a parameter  $\lambda \in \mathbb{R}$ , functional  $F_t(\mathbf{S}, \lambda)$  is a pseudo-bound for energy  $E(\mathbf{S})$  if there exists at least one  $\lambda'$  such that  $F_t(\mathbf{S}, \lambda')$  is an auxiliary function of  $E(\mathbf{S})$  at current solution  $\mathbf{S}_t$ .*

Instead of using an auxiliary function, one can optimize a family of pseudo-bounds that includes at least one proper bound. This guarantees that original functional  $E(\mathbf{S})$  decreases when the best solution is selected among the global minima for the whole family [56]. In the meanwhile, such pseudo-bounds may approximate  $E(\mathbf{S})$  better than a single auxiliary function, even though they come from the same class of sub-modular (globally optimizable) functionals. The experiments of [56] confirmed that pseudo-bounds significantly outperform the optimization quality obtained by a single auxiliary function in the context of several high-order

<sup>7</sup>Dhillion et al. [21] converts normalized cuts directly to  $k$ KM using a different kernel  $k' = \text{diag}(\mathcal{W}) \cdot A \cdot \text{diag}(\mathcal{W}) + \lambda \cdot \text{diag}(\mathcal{W})$ . To make  $k'$  psd one needs a different  $\lambda$  from the one that work for our kernel in (28).

segmentation functionals, e.g., entropy [58], Bhattacharyya measure [4] and KL divergence [5]<sup>8</sup>. If the pseudo-bounds are monotone w.r.t. parameter  $\lambda$ , we can find all global minima for the whole family in polynomial time via parametric max-flow algorithm [36]. This practical consideration is important when building a pseudo-bound family. For instance, [56] built pseudo-bounds by simply adding monotone unary term  $\lambda|\mathbf{S}|$  to a given auxiliary function. Here we follow a different approach for (25). As we will see next, our approach removes the need for computing expensive eigen-value decompositions.

**Proposition 4.** *The following function is a pseudo-bound over parameter  $\lambda$  for the general pairwise clustering formulation (25) with arbitrary matrix  $A$*

$$\begin{aligned}
 F_t(\mathbf{S}, \lambda) = & - \sum_{p \in \mathbf{S}} \frac{\sum_{q \in \mathbf{S}_t} w_p w_q (A_{pq} + A_{qp})}{\langle \mathbf{S}_t, W \rangle} \\
 & - \sum_{p \in \bar{\mathbf{S}}} \frac{\sum_{q \in \bar{\mathbf{S}}_t} w_p w_q (A_{pq} + A_{qp})}{\langle \bar{\mathbf{S}}_t, W \rangle} \\
 & + \langle \mathbf{S}, W \rangle \frac{\sum_{pq \in \mathbf{S}_t} w_p w_q (A_{pq} + A_{qp})}{2 \langle \mathbf{S}_t, W \rangle^2} \\
 & + \langle \bar{\mathbf{S}}, W \rangle \frac{\sum_{pq \in \bar{\mathbf{S}}_t} w_p w_q (A_{pq} + A_{qp})}{2 \langle \bar{\mathbf{S}}_t, W \rangle^2} \\
 & + \lambda \left( 2 - \frac{\langle \mathbf{S}, W \rangle}{\langle \mathbf{S}_t, W \rangle} - \frac{\langle \bar{\mathbf{S}}, W \rangle}{\langle \bar{\mathbf{S}}_t, W \rangle} \right) \quad (32)
 \end{aligned}$$

Furthermore, for any  $\lambda \geq -\lambda_0(A^W)$  functional  $F_t(\mathbf{S}, \lambda)$  is an auxiliary function for weighted AA energy (25).

*Proof.* See appendix A.  $\square$

Note that pseudo-bound (32) for  $\lambda = 0$  gives the bound in Proposition 1 in case of psd  $A$  such that  $\lambda_0(A^W) \geq 0$ .

Proposition 4 provides a pseudo-bound for the binary case of weighted AA. Pseudo bound  $F_t(\mathbf{S}, \lambda)$  consists of unary terms *monotonic* w.r.t  $\lambda$ . Therefore, any combination of  $F_t(\mathbf{S}, \lambda)$  with sub-modular regularization terms can be minimized for all  $\lambda$  in polynomial time via parametric max-flow [36]. This removes the need for evaluating explicitly  $\lambda_0(A^W)$  avoiding eigen-value decompositions. Pseudo-bound  $F_t(\mathbf{S}, \lambda)$  can also be used for weighted AA without any regularization. In this case neither max-flow nor monotonicity are needed. Indeed, a unary potential for each pixel in (32) changes its sign only once as parameter  $\lambda$  increases. It is enough to sort all critical values of  $\lambda$  changing at least one pixel in order to traverse all (at most  $1 + |\Omega|$ ) distinct solutions for pseudo bound (32) in a linear time.

The pseudo-bound in Proposition 4 could be easily written for the multi-label case. However, monotonicity is not

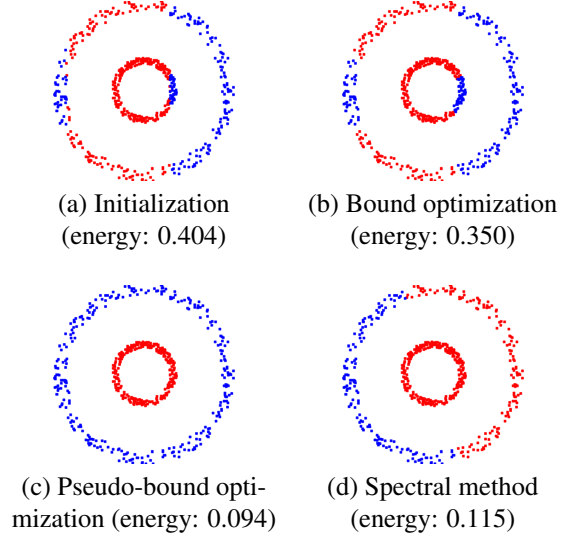


Figure 6: Normalized cut / weighted AA energy (31). This proof-of-the-concept example shows that our *pseudo-bound* optimization (c) is less sensitive to local minima compared to the standard  $k$ KM algorithm (bound optimizer) in (b). Our approach can compete with spectral methods [54] (d).

guaranteed. For additional regularization terms it is still possible to use  $\alpha$ -expansion [11] or other algorithms but the number of distinct solutions for all  $\lambda$  can not be linearly bounded. However, some easy fixes could be explored. For example, it is possible to consider restricted expansion moves limited to “monotone” subsets of pixels with either positive or negative unary potential with respect to  $\lambda$ .

Without regularization terms, monotonicity of the parametric unary pseudo-bound (32) is not essential. Similarly to the binary case discussed earlier, it is easy to check that the optimal label for each pixel changes at most  $K - 1$  times as  $\lambda$  increases<sup>9</sup>. Critical values of  $\lambda$  for all pixels can be sorted so that all (at most  $1 + (K - 1)|\Omega|$ ) distinct solutions for pseudo bound (32) can be explored in a linear time.

Detailed evaluation of pseudo-bound optimization based on (32) will be reported later. As a proof-of-the-concept, we included Figure 6 demonstrating only one synthetic binary clustering example. It uses standard normalized cut (weighted AA) energy (31) with Gaussian affinity and no additional regularization terms. Basic bound optimization ( $\lambda = 0$  in (32)) converges to a bad local minimum, while pseudo-bound optimization over all  $\lambda$  achieves a much better solution with lower energy. This toy example also shows that our pseudo-bound approach to pairwise clustering may compete with standard spectral relaxation methods [54].

Examples in later sections use bound (20) for color space clustering combined with spatial domain regularization.

<sup>8</sup>The segmentation functionals considered in [56] are completely different from the pairwise clustering energies we consider in this work

<sup>9</sup>The optimal value of a unary potential for each pixels is the lower envelope of  $K$  linear functions of  $\lambda$ , which has at most  $K - 1$  breakpoints.



#### 4. Parzen Analysis and Bandwidth Selection

This section discusses connections of  $k$ KM energy to Parzen densities providing probabilistic interpretations for our pairwise clustering approach. In particular, this section gives insights on bandwidth selection. We discuss extreme cases and analyze adaptive strategies. For simplicity, we mainly focus on Gaussian kernels, even though the analysis applies to other types of positive normalized kernels.

Note that standard Parzen density estimate for the distribution of data points within segment  $\mathbf{S}$  can be expressed using normalized Gaussian kernels [6, 26]

$$\mathcal{P}_k(I_p|\mathbf{S}) = \frac{\sum_{q \in \mathbf{S}} k(I_p, I_q)}{|\mathbf{S}|}. \quad (33)$$

It is easy to see that  $k$ KM energy (11) is exactly the following high-order Parzen density energy

$$E_k(\mathbf{S}) \stackrel{c}{=} - \sum_{p \in \mathbf{S}} \mathcal{P}_k(I_p|\mathbf{S}) - \sum_{p \in \bar{\mathbf{S}}} \mathcal{P}_k(I_p|\bar{\mathbf{S}}). \quad (34)$$

This probabilistic interpretation of  $k$ KM gives an additional point of view for comparing it with pKM clustering with log-likelihood energy (4). Instead of parametric ML models  $k$ KM uses Parzen density estimates. Another difference is absence of the log in (34). Omitting the log reduces the weight of low probability points, that is, outliers. In contrast, log-likelihoods in (4) are highly sensitive to outliers. To address this problem, pKM methods often use heuristics like mixing the desired probability model  $\mathcal{P}$  with a uniform distribution, e.g.  $\tilde{\mathcal{P}}(\cdot|\theta) := \epsilon + (1 - \epsilon)\mathcal{P}(\cdot|\theta)$ .

##### 4.1. Extreme bandwidth cases

Parzen energy (34) is also useful for analyzing two extreme cases of kernel bandwidth: large kernels approaching the data range and small kernels approaching the data resolution. This section analyses these two extreme cases.

**Large bandwidth and basic K-means:** Consider Gaussian kernels of large bandwidth  $\sigma$  approaching the data range. In this case Gaussian kernels  $k$  in (33) can be approximated (up to a scalar) by Taylor expansion  $1 - \frac{\|I_p - I_q\|^2}{2\sigma^2}$ . Then, Parzen density energy (34) becomes (up to a constant)

$$\frac{\sum_{pq \in \mathbf{S}} \|I_p - I_q\|^2}{2|\mathbf{S}|\sigma^2} + \frac{\sum_{pq \in \bar{\mathbf{S}}} \|I_p - I_q\|^2}{2|\bar{\mathbf{S}}|\sigma^2}$$

which is proportional to the pairwise formulation for the basic K-means or *variance criteria* in Tab.1A with Euclidean metric  $\|\cdot\|$ . That is,  $k$ KM for large bandwidth Gaussian kernels reduces to the basic K-means in the original data space instead of the high-dimensional embedding space.

In particular, this proves that as the bandwidth gets too large  $k$ KM loses its ability to find non-linear separation of

the clusters. This also emphasizes the well-known bias of basic K-means to equal size clusters [33, 8].

**Small bandwidth and Gini criterion:** Very different properties could be shown for the opposite extreme case of small bandwidth approaching data resolution. It is easy to approximate Parzen formulation of  $k$ KM energy (34) as

$$E_k(\mathbf{S}) \stackrel{c}{\approx} -|\mathbf{S}| \cdot \langle \mathcal{P}_k(\mathbf{S}), d_{\mathbf{s}} \rangle - |\bar{\mathbf{S}}| \cdot \langle \mathcal{P}_k(\bar{\mathbf{S}}), d_{\bar{\mathbf{s}}} \rangle \quad (35)$$

where  $\mathcal{P}_k(\mathbf{S})$  is kernel-based density (33) and  $d_{\mathbf{s}}$  is a “true” density for intensities in  $\mathbf{S}$ . Approximation (35) follows directly from the same Monte-Carlo estimation argument given earlier below Eq. (5) in Sec.1.1 with the only difference being  $f = -\mathcal{P}_k(\mathbf{S})$  instead of  $-\log \mathcal{P}(\theta_{\mathbf{S}})$ .

If kernels have small bandwidth optimal for accurate Parzen density estimation<sup>10</sup> we get  $\mathcal{P}_k(\mathbf{S}) \approx d_{\mathbf{s}}$  further reducing (35) to approximation

$$\stackrel{c}{\approx} -|\mathbf{S}| \cdot \langle d_{\mathbf{s}}, d_{\mathbf{s}} \rangle - |\bar{\mathbf{S}}| \cdot \langle d_{\bar{\mathbf{s}}}, d_{\bar{\mathbf{s}}} \rangle$$

that proves the following property.

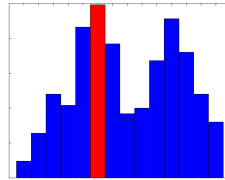
**Property 1.** Assume small bandwidth Gaussian kernels optimal for accurate Parzen density estimation. Then kernel K-means energy (34) can be approximated by the standard Gini criterion for clustering [12]:

$$E_G(\mathbf{S}) := |\mathbf{S}| \cdot G(\mathbf{S}) + |\bar{\mathbf{S}}| \cdot G(\bar{\mathbf{S}}) \quad (36)$$

where  $G(\mathbf{S})$  is the Gini impurity for the data points in  $\mathbf{S}$

$$G(\mathbf{S}) := 1 - \langle d_{\mathbf{s}}, d_{\mathbf{s}} \rangle \equiv 1 - \int_x d_{\mathbf{s}}^2(x) dx. \quad (37)$$

Similarly to entropy, *Gini impurity*  $G(\mathbf{S})$  can be viewed as a measure of sparsity or “peakedness” for continuous or discrete distributions. Both Gini and entropy clustering criteria are widely used for decision trees [12, 42]. In this discrete context Breiman [12] analyzed theoretical



properties of Gini criterion (36) for the case of histograms  $\mathcal{P}_h$  where  $G(\mathbf{S}) = 1 - \sum_x \mathcal{P}_h(x|\mathbf{S})^2$ . He proved that the minimum of the Gini criterion is achieved by sending all data points within the highest-probability bin to one cluster and the remaining data points to the other cluster, see the color encoded illustration above. We extend Breiman’s result to the continuous Gini criterion (36)-(37).

**Theorem 1. (Gini Bias)** Let  $d_{\Omega}$  be a continuous probability density function over domain  $\Omega \subseteq \mathcal{R}^n$  defining conditional density  $d_{\mathbf{s}}(x) := d_{\Omega}(x|x \in \mathbf{S})$  for any non-empty subset

<sup>10</sup>Bandwidth near inter-point distances avoids density oversmoothing.

$\mathbf{S} \subset \Omega$ . Then, continuous version of Gini clustering criterion (36) achieves its optimal value at the partitioning of  $\Omega$  into regions  $\mathbf{S}$  and  $\bar{\mathbf{S}} = \Omega \setminus \mathbf{S}$  such that

$$\mathbf{S} = \arg \max_x d_\Omega(x).$$

*Proof.* See Appendix B and Proposition 5.  $\square$

The bias to small dense clusters is practically noticeable for small bandwidth kernels, see Fig.8(d). Similar empirical bias to tight clusters was also observed in the context of average association (11) in [54]. As kernel gets wider the continuous Parzen density (33) no longer approximates the true distribution  $d_s$  and Gini criterion (36) is no longer valid as an approximation for  $k$ KM energy (34). In practice, *Gini bias* gradually disappears as bandwidth gets wider. This also agrees with the observations for wider kernel in average association [54]. As discussed earlier, in the opposite extreme case when bandwidth get very large (approaching data range)  $k$ KM converges to basic K-means or *variance criterion*, which has very different properties. Thus, kernel K-means properties strongly depend on the bandwidth.

The extreme cases for kernel K-means, *i.e.* Gini and variance criteria, are useful to know when selecting kernels. Variance criteria for clustering has bias to equal cardinality segments [33, 8]. In contrast, Gini criteria has bias to small dense clusters (Theorem 1). To avoid these biases kernel K-means should use kernels of width that is neither too small nor too large. Our experiments compare different strategies with fixed and adaptive-width kernels (Sec.4.2). Equivalence of kernel-K-means to many standard clustering criteria such as *average distortion*, *average association*, *normalized cuts*, *etc.* (see Sec.1.2) also suggest kernel selection strategies based on practices in the prior literature.

## 4.2. Adaptive kernels via Nash embedding

As discussed in Sec.4.1, kernel width should neither be too small nor too large. We propose adaptive kernels designed to equalize the density in highly dense regions in the color space. The following equation interprets adaptive Gaussian kernels via Riemannian distances in the color space (left picture in Fig.7)

$$\begin{aligned} k_p(I_p, I_q) &= e^{\frac{-\|I_p - I_q\|^2}{2\sigma_p^2}} \\ &= e^{\frac{-(I_p - I_q)^T \Sigma_p^{-1} (I_p - I_q)}{2}}. \end{aligned}$$

According to Nash embedding theorem [46], this Riemannian color space can be isometrically embedded into a Euclidean space, so that the last expression above is equal to

$$= e^{\frac{-\|I'_p - I'_q\|^2}{2}} = k(I'_p, I'_q)$$

where  $k$  is a fixed-width Gaussian kernel in the new transformed space (right picture in Fig.7). Thus, non-normalized

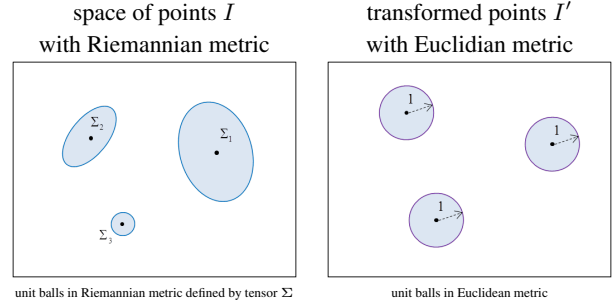


Figure 7: *Nash embedding*: adaptive non-normalized Gaussian kernels define isometric transformation of the color space modifying density. Ellipsoids are mapped to balls.

Gaussian kernels of adaptive width  $\sigma_p$  (or covariance matrix  $\Sigma_p$ , in general) define some color space transformation, *Nash embedding*, that locally stretches or shrinks the space. After this transformation, clustering is done using a fixed (homogeneous) Gaussian kernel of constant width.

Figure 7 helps to illustrate how Nash embedding changes the color space density. The number of points in a unit (Euclidean) ball neighborhood in the transformed space is equal to the number of points in the corresponding unit (Riemannian) ball in the original space:

$$K = d' \cdot V_1 = d \cdot V_\sigma$$

where  $d$  and  $d'$  are local densities in the original and transformed spaces. Thus, kernel width  $\sigma_p$  can be selected adaptively based on any desired transformation of density  $d'(d)$  according to formula

$$\sigma_p \sim \sqrt[n]{\frac{d'(d_p)}{d_p}} \quad (38)$$

where  $d_p := d(I_p)$  is an observed local density for points in the color space. This local density can be evaluated using any common estimator, *e.g.* Parzen approach gives

$$d(I_p) \sim \sum_q \frac{1}{\Delta_q^n} \cdot e^{\frac{-\|I_p - I_q\|^2}{2\Delta_q^2}} \quad (39)$$

where  $\Delta_q$  could be adaptive or fixed  $\Delta_q = \text{const}$ , according to any standard technique for density estimation [6].

To address Breiman bias one can use density equalizing transforms  $d'(d) = \text{const}$  or  $d' = \frac{1}{\alpha} \log(1 + \alpha d)$ , which even up the highly dense parts of the color space. Formula (38) works for any target transform  $d'(d)$ . Once adaptive kernels  $\sigma_p$  are chosen, Nash theory also allows to obtain empirical scatter plots  $d'(d)_\Omega := \{(d'(I'_p), d(I_p)) | p \in \Omega\}$ , for example, to compare it with the selected “theoretical”

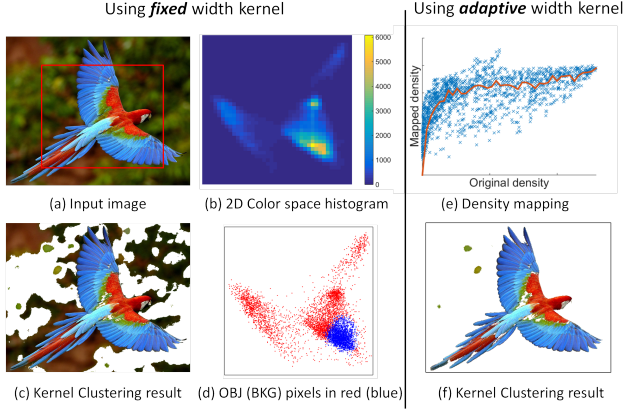


Figure 8: (a)-(d): Breiman bias for fixed (small) kernel. (e) Empirical density transform for adaptive kernels (38) with  $d'(d) = \text{const}$ . Color space density equalization counters Breiman bias. (f) Segmentation for adaptive kernels.

plot  $d'(d)$ . Estimates  $d(I_p)$  are provided in (39) and the density estimate for Nash embedding are

$$d'(I'_p) \sim \sum_q e^{-\frac{\|I'_p - I'_q\|^2}{2}} = \sum_q e^{-\frac{\|I_p - I_q\|^2}{2\sigma_q^2}}. \quad (40)$$

Note the difference between empirical density estimates for  $d'$  in (40) and  $d$  in (39): the former uses the sum of *non-normalized* kernels of selected adaptive width  $\sigma_q$  in (38) and the latter is the sum of *normalized* kernels of width  $\Delta_q$  based on chosen density estimator. While parameter  $\sigma_q$  directly controls the density transformation,  $\Delta$  plays a fairly minor role concerning the quality of estimating density  $d$ .

Figure 8(e) illustrates the empirical density mapping  $d'(d)_\Omega$  induced by adaptive kernels (38) for  $d'(d) = \text{const}$ . Notice a density-equalization effect within high density areas in the color space addressing the Breiman bias.

## 5. Experiments

**Efficient evaluation of bounds  $A_t(\mathbf{S})$ :** As mentioned in Sec. 2, deriving the coefficients of upper bound  $A_t(\mathbf{S})$  in (20) for each iteration is of  $O(|\Omega|^2)$  time complexity. Here we give an efficient way of bound evaluation. Notice that the most expensive part of deriving the linear bound  $A_t(\mathbf{S})$  is to compute  $\sum_{q \in S_t} k_{pq}$  and  $\sum_{q \in S_t} k_{pq}$  for each  $p \in \Omega$ .

For computing  $\sum_{q \in S_t} k_{pq}$ , in the case of fixed width Gaussian kernel  $k_{pq}$ , we resort to fast approximate dense filtering method in [48], which takes  $O(|\Omega|)$  time. Also notice that the time complexity of the approach in [48] grows exponentially with data dimension  $D$ . A better approach for high-dimensional dense filtering is proposed in [1], which is of time  $O(|\Omega| \times D)$ . We stick to [48] for low-dimensional color space in our experiments. For general kernel (adaptive

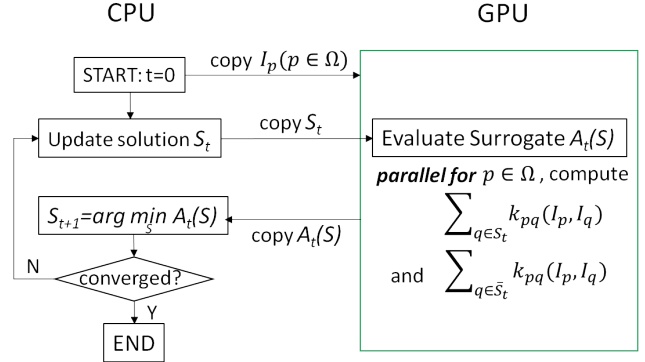


Figure 9: Efficient Kernel K-means with GPU.

width Gaussian kernel), we developed the GPU framework in Fig. 9. Evaluation of surrogates is conducted on GPU, while the CPU optimizes the bounds, updates solutions and checks convergence. Using this framework, we achieved empirical speedup close to the number of cores in GPU.

**Implementation details:** LAB color space is used for all algorithms. For GrabCut, we used histogram-based probability model, as is common in the literature [58, 39]. For contrast-sensitive regularization, we use standard penalty  $w_{pq} = \frac{1}{d_{pq}} e^{-0.5\|I_p - I_q\|_2^2/\beta}$ , where  $\beta$  is the average of  $\|I_p - I_q\|_2^2$  over a 8-connected neighborhood and  $d_{pq}$  is the distance between pixels  $p$  and  $q$  in the image plane. We set  $w_{pq} = \frac{1}{d_{pq}}$  for length regularization. We choose sampling rate as half of kernel width  $\sigma$  for Bilateral Grid in [48].

We evaluated our kernel-based method (fixed or adaptive kernel width) in the context of interactive segmentation, and compared with the commonly used GrabCut algorithm [50]. The adaptive kernel width is determined by (38) where we choose target density  $d'(d)$  to be a constant, which we found to be working well in practice compared to other density mapping such as  $d' = \frac{1}{\alpha} \log(1 + \alpha d)$ . We experiment with both (i) contrast-sensitive edge regularization, (ii) length regularization and (iii) color clustering (i.e., no regularization) so as to assess to what extent the algorithms benefit from regularization. We further report results on the GrabCut dataset of 50 images.

### 5.1. Robustness to regularization weight

We first run all algorithms without smoothness. Then, we experiment with several values of  $\lambda$  for the contrast-sensitive edge term. In the experiments of Fig. 10 (a) and (b), we used the yellow boxes as initialization. For a clear interpretation of the results, we did not use any additional hard constraint. Without smoothness, our kernel-based method yielded much better results than model fitting. Regularization significantly benefited the latter, as the decreasing blue curve in (a) indicates. For instance, in the

case of the zebra image, model fitting yielded a plausible segmentation when assisted with a strong regularization. However, in the presence of noisy edges and clutter, as is the case of the chair image in (b), regularization did not help as much. Notice that, for small regularization weights, our method is substantially better than model fitting. Also, notice the performance of our method is less dependent on regularization weight; therefore, it does not require fine tuning of  $\lambda$ .

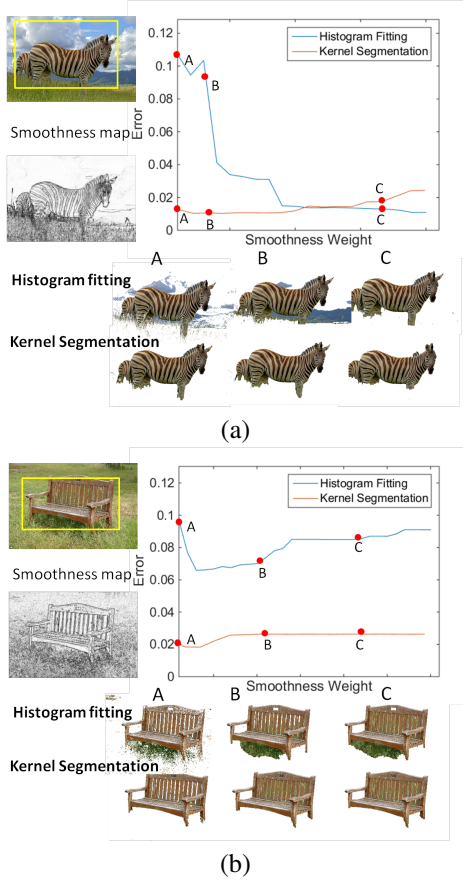


Figure 10: Illustration of robustness to smoothness weight.

## 5.2. Results on the GrabCut Database

We report results on the GrabCut Database (50 images with ground truth) using the bounding boxes provided in [40]. For each image the error is evaluated by the percentage of mis-labeled pixels w.r.t ground truth, and we computed the average error over the dataset.

Fig. 11 and Tab. 3 show the results for the GrabCut dataset. We test different smoothness weights, and plot the error curves for different methods<sup>11</sup>; see Fig. 11. The

<sup>11</sup>The smoothness weights for different energies are not directly comparable; Fig. 11 shows all the curves for better visualization.

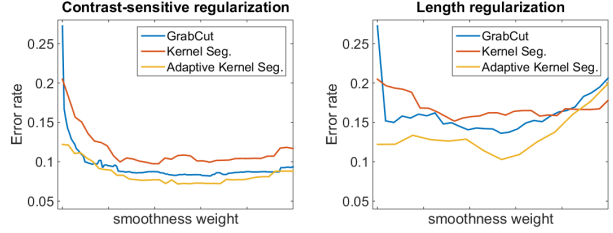


Figure 11: Average error. vs. regularization weights for different algorithms on the GrabCut dataset.

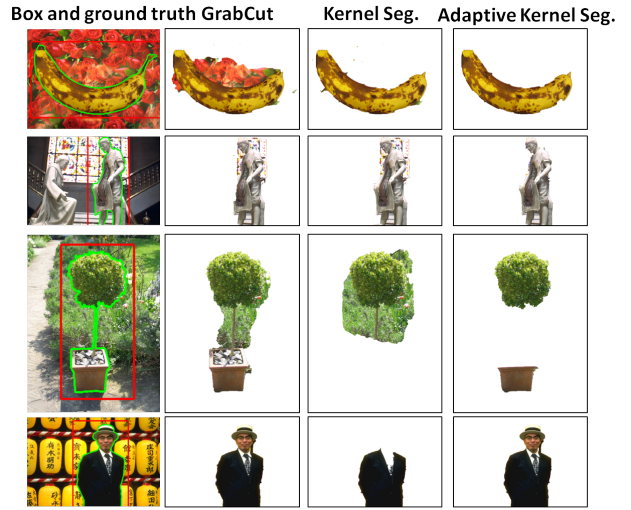


Figure 12: Sample results from the dataset using GrabCut and our kernel approach (fixed & adaptive widths).

best error each method obtained is reported in Tab. 3. For contrast-sensitive regularization, GrabCut achieves reasonable results (8.2% error rate). However, with length regularization, which is less informative about edges, GrabCut gives much higher error 13.6%. Without any regularization, GrabCut yields a significantly higher error rate of 27.2%, whereas our adaptive kernel segmentation achieved 12.2%, an error less than half of GrabCut's. In the case of contrast-sensitive regularization, our method outperformed GrabCut (7.1% vs. 8.2%), but this improvement is more substantial in the other less informative regularization settings.

Fig. 12 depicts some results of the algorithms. The top row shows a failure case of GrabCut, where the solution aligns with strong edges. The second row shows a challenging image for which our adaptive kernel method works well. The third and fourth rows depict failure cases of fixed-width kernel segmentation, where image segments of uniform color are separated; see green bush and black suit. This can be explained by the Breiman's bias we discussed earlier. Our adaptive kernel approach managed such bias giving better segmentation.



| Error (%)                      | GrabCut | Kernel Segmentation | Adaptive Kernel Segmentation |
|--------------------------------|---------|---------------------|------------------------------|
| no smoothness regul.           | 27.2    | 20.4                | <b>12.2</b>                  |
| with length regul.             | 13.6    | 15.1                | <b>10.2</b>                  |
| with contrast-sensitive regul. | 8.2     | 9.7                 | <b>7.1</b>                   |

Table 3: Error rates of the algorithms with or without smoothness regularization in the energy.

## APPENDIX A

In this appendix we prove Proposition 1 in the case of a weighted (more general) version of the  $k$ KM formulation in (11):

$$E_k^W(\mathbf{S}) = -\frac{\sum_{pq \in \mathbf{S}} w_p w_q k_{pq}}{\langle \mathbf{S}, W \rangle} - \frac{\sum_{pq \in \bar{\mathbf{S}}} w_p w_q k_{pq}}{\langle \bar{\mathbf{S}}, W \rangle}. \quad (\text{A-1})$$

where  $W := [w_p]$  denotes a vector of some given positive weights  $w_p$ . We also prove proposition 4.

**Proof of proposition 1:** Let us consider the following function for a given  $\mathbf{S}$ :

$$F_{\mathbf{S}}^W(c_1, c_2) = \sum_{p \in \mathbf{S}} w_p \|\phi(I_p) - c_1\|^2 + \sum_{p \in \bar{\mathbf{S}}} w_p \|\phi(I_p) - c_2\|^2 \quad (\text{A-2})$$

This function is convex w.r.t variables  $c_1$  and  $c_2$ . Therefore its global minima are reached at stationary points  $c_1^*$  and  $c_2^*$  verifying  $\frac{\partial F_{\mathbf{S}}^W}{\partial c_1^*} = \frac{\partial F_{\mathbf{S}}^W}{\partial c_2^*} = 0$ . It is easy to check these necessary conditions for a minimum of  $F_{\mathbf{S}}^W$  are verified if and only if:

$$\begin{aligned} c_1^* &= \frac{\sum_{q \in \mathbf{S}} w_q \phi(I_q)}{\langle \mathbf{S}, W \rangle} \\ c_2^* &= \frac{\sum_{q \in \bar{\mathbf{S}}} w_q \phi(I_q)}{\langle \bar{\mathbf{S}}, W \rangle} \end{aligned} \quad (\text{A-3})$$

where  $\langle \mathbf{S}, W \rangle = \sum_{p \in \mathbf{S}} w_p$ . Now notice the following:

$$\begin{aligned} F_{\mathbf{S}}^W(c_1^*, c_2^*) &= C(\Omega) + E_k^W(\mathbf{S}) \\ &\leq F_{\mathbf{S}}^W(c_1, c_2) \quad \forall c_1, c_2 \end{aligned} \quad (\text{A-4})$$

where  $C(\Omega) = \sum_{p \in \Omega} w_p k_{pp}$  is a constant independent of segmentation  $\mathbf{S}$ . The inequality in (A-4) is due to the fact that solution  $\{c_1^*, c_2^*\}$  is the global minimum for  $F_{\mathbf{S}}^W(c_1, c_2)$ . The equality in the first line comes from expanding the Euclidean distances in  $F_{\mathbf{S}}^W(c_1^*, c_2^*)$  and replacing dot products  $\langle \phi(I_p), \phi(I_q) \rangle$  by kernels  $k_{pq}$ . This yields the following bounds on the weighted  $k$ KM formulation in (A-1):

$$E_k^W(\mathbf{S}) \leq F_{\mathbf{S}}^W(c_1, c_2) - C(\Omega) \quad \forall c_1, c_2 \quad (\text{A-5})$$

Given current solution  $\mathbf{S}_t$ , we apply inequality (A-5) to  $c_1 = \mu_{\mathbf{S}_t} = \frac{\sum_{q \in \mathbf{S}_t} w_q \phi(I_q)}{\langle \mathbf{S}_t, W \rangle}$  and  $c_2 = \mu_{\bar{\mathbf{S}}_t} = \frac{\sum_{q \in \bar{\mathbf{S}}_t} w_q \phi(I_q)}{\langle \bar{\mathbf{S}}_t, W \rangle}$ :

$$\begin{aligned} E_k^W(\mathbf{S}) &\leq F_{\mathbf{S}}^W(\mu_{\mathbf{S}_t}, \mu_{\bar{\mathbf{S}}_t}) - C(\Omega) \\ &= \sum_{p \in \mathbf{S}} w_p \left\| \phi(I_p) - \frac{\sum_{q \in \mathbf{S}_t} w_q \phi(I_q)}{\langle \mathbf{S}_t, W \rangle} \right\|^2 \\ &\quad + \sum_{p \in \bar{\mathbf{S}}} w_p \left\| \phi(I_p) - \frac{\sum_{q \in \bar{\mathbf{S}}_t} w_q \phi(I_q)}{\langle \bar{\mathbf{S}}_t, W \rangle} \right\|^2 - C(\Omega) \\ &= -2 \sum_{p \in \mathbf{S}} \frac{\sum_{q \in \mathbf{S}_t} w_p w_q k_{pq}}{\langle \mathbf{S}_t, W \rangle} \\ &\quad - 2 \sum_{p \in \bar{\mathbf{S}}} \frac{\sum_{q \in \bar{\mathbf{S}}_t} w_p w_q k_{pq}}{\langle \bar{\mathbf{S}}_t, W \rangle} \\ &\quad + \langle \mathbf{S}, W \rangle \frac{\sum_{pq \in \mathbf{S}_t} w_p w_q k_{pq}}{\langle \mathbf{S}_t, W \rangle^2} \\ &\quad + \langle \bar{\mathbf{S}}, W \rangle \frac{\sum_{pq \in \bar{\mathbf{S}}_t} w_p w_q k_{pq}}{\langle \bar{\mathbf{S}}_t, W \rangle^2} \end{aligned} \quad (\text{A-6})$$

It is easy to verify that this bound is equal to  $E_k^W$  at  $\mathbf{S}_t$ . This proves proposition 1. Furthermore, from the second and third lines of (A-6), one can easily see that the standard point re-assignment step in kernel  $k$ -means (Step II in proposition 2) optimizes globally the auxiliary function.

**Proof of proposition 4:** It suffices to see the following:

$$\begin{aligned} \text{For psd matrix } k &= \frac{A + A^T}{2} + \lambda \cdot \text{diag}(W), \text{ we have} \\ E_A^W(\mathbf{S}) &= E_k^W(\mathbf{S}) + 2\lambda \end{aligned} \quad (\text{A-7})$$

Then, because  $k$  is psd  $\forall \lambda \geq -\lambda_0(A^W)$ , we can apply the bound in (A-6) to the  $E_k^W$  that appears in (A-7). This yields:

$$E_A^W(\mathbf{S}) \leq F_t(\mathbf{S}, \lambda) \quad \forall \lambda \geq -\lambda_0(A^W) \quad (\text{A-8})$$

It is easy to check that  $E_A^W(\mathbf{S}_t) \leq F_t(\mathbf{S}_t, \lambda) \forall \lambda$ .

## APPENDIX B (proof of Gini Bias Theorem 1)

Let  $d_\Omega$  be a continuous probability density function over domain  $\Omega \subseteq \mathcal{R}^n$  defining conditional density

$$d_{\mathbf{S}}(x) := d_\Omega(x|x \in \mathbf{S}) \quad (\text{B-1})$$

for any non-empty subset  $\mathbf{S} \subset \Omega$  and expectation

$$\mathbf{E}z := \int z(x)d_\Omega(x)dx$$

for any function  $z : \Omega \rightarrow \mathcal{R}^1$ .

Suppose  $\Omega$  is partitioned into two sets  $\mathbf{S}$  and  $\bar{\mathbf{S}}$  such that  $\mathbf{S} \cup \bar{\mathbf{S}} = \Omega$  and  $\mathbf{S} \cap \bar{\mathbf{S}} = \emptyset$ . Note that  $\mathbf{S}$  here and in the statement of Theorem 1 is not a discrete set of observations, which is what  $\mathbf{S}$  means in the rest of the paper. Theorem 1 states a property of a fully continuous version of Gini criterion (36) that follows from an additional application of Monte-Carlo estimation allowing to replace discrete set cardinality  $|\mathbf{S}|$  by probability  $w$  of a continuous subset  $\mathbf{S}$

$$w := \int_{\mathbf{S}} d_\Omega(x)dx = \int d_\Omega(x) \cdot [x \in \mathbf{S}]dx = \mathbf{E}[x \in \mathbf{S}].$$

Then, minimization of  $E_G(\mathbf{S})$  in (36) corresponds to maximization of the following objective function

$$L(\mathbf{S}) := w \int d_{\mathbf{S}}^2(x)dx + (1-w) \int d_{\bar{\mathbf{S}}}^2(x)dx. \quad (\text{B-2})$$

Note that conditional density  $d_{\mathbf{S}}$  in (B-1) can be written as

$$d_{\mathbf{S}}(x) = d_\Omega(x) \cdot \frac{[x \in \mathbf{S}]}{w} \quad (\text{B-3})$$

where  $[\cdot]$  is an indicator function. Eqs. (B-3) and (B-2) give

$$L(\mathbf{S}) = \frac{1}{w} \int d_\Omega^2(x)[x \in \mathbf{S}]dx + \frac{1}{1-w} \int d_\Omega^2(x)[x \in \bar{\mathbf{S}}]dx.$$

Introducing notation

$$I := [x \in \mathbf{S}] \quad \text{and} \quad F := d_\Omega(x)$$

allows to further rewrite objective function  $L(\mathbf{S})$  as

$$L(\mathbf{S}) = \frac{\mathbf{E}IF}{\mathbf{E}I} + \frac{\mathbf{E}F(1-I)}{1-\mathbf{E}I}.$$

Without loss of generality assume that  $\frac{\mathbf{E}F(1-I)}{1-\mathbf{E}I} \leq \frac{\mathbf{E}FI}{\mathbf{E}I}$  (the opposite case would yield a similar result). We now need the following lemma.

**Lemma 1.** *Let  $a, b, c, d$  be some positive numbers, then*

$$\frac{a}{b} \leq \frac{c}{d} \implies \frac{a}{b} \leq \frac{a+c}{b+d} \leq \frac{c}{d}.$$

*Proof.* Use reduction to a common denominator.  $\square$

Lemma 1 implies inequality

$$\frac{\mathbf{E}F(1-I)}{1-\mathbf{E}I} \leq \mathbf{E}F \leq \frac{\mathbf{E}FI}{\mathbf{E}I} \quad (\text{B-4})$$

which is needed to prove the Proposition below.

**Proposition 5. (Gini-bias)** *Assume that subset  $\mathbf{S}_\varepsilon \subset \Omega$  is*

$$\mathbf{S}_\varepsilon := \{x : d_\Omega(x) \geq \sup_x d_\Omega(x) - \varepsilon\}. \quad (\text{B-5})$$

*Then*

$$\sup_{\mathbf{S}} L(\mathbf{S}) = \lim_{\varepsilon \rightarrow 0} L(\mathbf{S}_\varepsilon) = \mathbf{E}d_\Omega + \sup_x d_\Omega(x). \quad (\text{B-6})$$

*Proof.* Due to monotonicity of expectation we have

$$\frac{\mathbf{E}FI}{\mathbf{E}I} \leq \frac{\mathbf{E}(I \sup_x d_\Omega(x))}{\mathbf{E}I} = \sup_x d_\Omega(x). \quad (\text{B-7})$$

Then (B-4) and (B-7) imply

$$L(\mathbf{S}) = \frac{\mathbf{E}FI}{\mathbf{E}I} + \frac{\mathbf{E}F(1-I)}{1-\mathbf{E}I} \leq \sup_x d_\Omega(x) + \mathbf{E}F. \quad (\text{B-8})$$

That is, the right part of (B-6) is an upper bound for  $L(\mathbf{S})$ .

Let  $I_\varepsilon \equiv [x \in \mathbf{S}_\varepsilon]$ . It is easy to check that

$$\lim_{\varepsilon \rightarrow 0} \frac{\mathbf{E}F(1-I_\varepsilon)}{1-\mathbf{E}I_\varepsilon} = \mathbf{E}F. \quad (\text{B-9})$$

Definition (B-5) also implies

$$\lim_{\varepsilon \rightarrow 0} \frac{\mathbf{E}FI_\varepsilon}{\mathbf{E}I_\varepsilon} \geq \lim_{\varepsilon \rightarrow 0} \frac{\mathbf{E}(\sup_x d_\Omega(x) - \varepsilon)I_\varepsilon}{\mathbf{E}I_\varepsilon} = \sup_x d_\Omega(x).$$

This result and (B-7) conclude that

$$\lim_{\varepsilon \rightarrow 0} \frac{\mathbf{E}FI_\varepsilon}{\mathbf{E}I_\varepsilon} = \sup_x d_\Omega(x). \quad (\text{B-10})$$

Finally, the limits in (B-9) and (B-10) imply

$$\begin{aligned} \lim_{\varepsilon \rightarrow 0} L(\mathbf{S}_\varepsilon) &= \lim_{\varepsilon \rightarrow 0} \frac{\mathbf{E}F(1-I_\varepsilon)}{1-\mathbf{E}I_\varepsilon} + \lim_{\varepsilon \rightarrow 0} \frac{\mathbf{E}FI_\varepsilon}{\mathbf{E}I_\varepsilon} \\ &= \mathbf{E}d_\Omega + \sup_x d_\Omega(x). \end{aligned}$$

This equality and bound (B-8) prove (B-6).  $\square$

## APPENDIX C (K-modes and mean shift)

Here we discuss some extra points about *K-modes* and standard *mean-shift* [25, 16, 18]. First of all, note that *K-modes* energy (18) follows from a weak *kKM* approach (Sec.1.2) for arbitrary positive normalized kernels. Such kernels define different Parzen densities, but they all lead to

energy (18) where optimal  $\mu_s$  and  $\mu_{\bar{s}}$  are modes of the corresponding densities. Different kernels give different modes.

Many optimization methods can be used for K-modes energy. For example, it is possible to use iterative (block-coordinate descent) approach typical of K-means methods: one step reclusters points and the other step locally refine the modes, *e.g.* using mean-shift operation [52]. For better optimization, local refinement of the mode in each cluster can be replaced by the best mode search tracing all points within each cluster using mean-shift. RANSAC-like sampling procedure can be used for some compromise between speed and quality. It is also possible to use exhaustive search for the strongest mode in each cluster over observed discrete features and then locally refine each cluster's mode with mean-shift.

It is also interesting that discrete version of K-modes for histograms [30, 15] define mode  $\mu = (\mu^1, \dots, \mu^j, \dots)$  as a combination of *marginal modes* for all attributes or dimensions  $j$ . Implicitly, they use distortion  $\|\cdot\|_k$  for discrete kernel  $k(x, y) = \sum_j [x^j = y^j]$  where  $[\cdot]$  are *Iverson brackets*. Marginal modes could be useful for aggregating sparse high-dimensional data.

Analogously, we can also define a continuous kernel for *marginal modes* as

$$k(x, y) = \sum_j e^{-\frac{(x^j - y^j)^2}{2\sigma^2}}. \quad (\text{C-1})$$

Note that this is different from the standard Gaussian kernel

$$e^{-\frac{\|x - y\|^2}{2\sigma^2}} = \prod_j e^{-\frac{(x^j - y^j)^2}{2\sigma^2}},$$

which leads to regular modes energy (18). It is easy to check that kernel (C-1) corresponds to weak  $k$ KM energy

$$\begin{aligned} & - \sum_j \sum_{p \in \mathbf{S}} e^{-\frac{(I_p^j - \mu_s^j)^2}{2\sigma^2}} - \sum_j \sum_{p \in \bar{\mathbf{S}}} e^{-\frac{(I_p^j - \mu_{\bar{s}}^j)^2}{2\sigma^2}} \\ & = - \sum_j \mathcal{P}_k^j(\mu_s^j | \mathbf{S}) - \sum_j \mathcal{P}_k^j(\mu_{\bar{s}}^j | \bar{\mathbf{S}}) \end{aligned}$$

where  $\mathcal{P}_k^j$  is a marginal Parzen density for dimension  $j$ .

## Acknowledgements

We would like to thank Carl Olsson (Lund University) for highly stimulating discussions and useful feedback at different stages of the project. Anders Eriksson (Lund University) gave us helpful advice on related work. We also thank Jianbo Shi for his feedback and for his spectral-relaxation optimization code for normalized cuts.

## References

- [1] A. Adams, J. Baek, and M. A. Davis. Fast high-dimensional filtering using the permutohedral lattice. *Computer Graphics Forum*, 29(2):753–762, 2010. 15
- [2] I. B. Ayed, A. Mitiche, and Z. Belhadj. Multiregion level set partitioning of synthetic aperture radar images. *IEEE Transactions on Pattern Analysis and Machine Intelligence (PAMI)*, 27(5):793–800, 2005. 2, 3
- [3] S. Basu, M. Bilenko, and R. J. Mooney. A probabilistic framework for semi-supervised clustering. In *International Conference on Knowledge Discovery and Data Mining (KDD)*, pages 1601–1608, August 2004. 3
- [4] I. Ben Ayed, H.-M. Chen, K. Punithakumar, I. Ross, and S. Li. Graph cut segmentation with a global constraint: Recovering region distribution via a bound of the bhattacharyya measure. In *CVPR*, pages 3288–3295, 2010. 12
- [5] I. Ben Ayed, L. Gorelick, and Y. Boykov. Auxiliary cuts for general classes of higher order functionals. In *IEEE conference on Computer Vision and Pattern Recognition (CVPR)*, pages 1304–1311, Portland, Oregon, June 2013. 12
- [6] C. M. Bishop. *Pattern Recognition and Machine Learning*. Springer, August 2006. 13, 14
- [7] A. Blake and A. Zisserman. *Visual Reconstruction*. Cambridge, 1987. 1
- [8] Y. Boykov, H. Isack, C. Olsson, and I. B. Ayed. Volumetric Bias in Segmentation and Reconstruction: Secrets and Solutions. In *arXiv:1505.00218*, May 2015. 9, 13, 14
- [9] Y. Boykov and M.-P. Jolly. *Interactive graph cuts* for optimal boundary & region segmentation of objects in N-D images. In *ICCV*, volume I, pages 105–112, July 2001. 1, 10
- [10] Y. Boykov and V. Kolmogorov. An experimental comparison of min-cut/max-flow algorithms for energy minimization in vision. *IEEE Transactions on Pattern Analysis and Machine Intelligence*, 26(9):1124–1137, 2004. 10
- [11] Y. Boykov, O. Veksler, and R. Zabih. Fast approximate energy minimization via graph cuts. *IEEE transactions on Pattern Analysis and Machine Intelligence*, 23(11):1222–1239, November 2001. 12
- [12] L. Breiman. Technical note: Some properties of splitting criteria. *Machine Learning*, 24(1):41–47, 1996. 4, 9, 13
- [13] M. A. Carreira-Perpinan and W. Wang. The K-Modes Algorithm for Clustering. In *arXiv:1304.6478v1 [cs.LG]*, April 2013. 2, 8
- [14] T. Chan and L. Vese. Active contours without edges. *IEEE Trans. Image Processing*, 10(2):266–277, 2001. 1, 2, 8, 9
- [15] A. Chaturvedi, P. E. Green, and J. D. Carroll. K-modes clustering. *Journal of Classification*, 18(1):35–55, 2001. 8, 19
- [16] Y. Cheng. Mean shift, mode seeking, and clustering. *IEEE Transactions on Pattern Analysis and Machine Intelligence (PAMI)*, 17(8):790–799, 1995. 9, 18
- [17] R. Chitta, R. Jin, T. C. Havens, and A. K. Jain. Scalable kernel clustering: Approximate kernel k-means. In *KDD*, pages 895–903, 2011. 4
- [18] D. Comaniciu and P. Meer. Mean shift: a robust approach toward feature space analysis. *IEEE Transactions on Pattern Analysis and Machine Intelligence (PAMI)*, 24(5):603–619, 2002. 8, 9, 18

- [19] I. Cox, S. Rao, and Y. Zhong. “Ratio Regions”: A Technique for Image Segmentation. In *International Conference on Pattern Recognition (ICPR)*, pages 557–564, 1996. 6
- [20] A. Delong, A. Osokin, H. Isack, and Y. Boykov. Fast Approximate Energy Minimization with Label Costs. *International Journal of Computer Vision (IJCV)*, 96(1):1–27, January 2012. 1, 2, 3, 8, 9
- [21] I. Dhillon, Y. Guan, and B. Kulis. Weighted graph cuts without eigenvectors: A multilevel approach. *IEEE Transactions on Pattern Analysis and Machine Learning (PAMI)*, 29(11):1944–1957, November 2007. 5, 6, 7, 10, 11
- [22] I. S. Dhillon, Y. Guan, and B. Kulis. Kernel k-means, spectral clustering and normalized cuts. In *KDD*, pages 551–556, 2004. 4, 5, 6, 7, 8, 10, 11
- [23] R. Duda, P. Hart, and D. Stork. *Pattern classification*. John Wiley & Sons, 2001. 6
- [24] A. Eriksson, C. Olsson, and F. Kahl. Normalized cuts revisited: A reformulation for segmentation with linear grouping constraints. *Journal of Mathematical Imaging and Vision*, 39(1):45–61, 2011. 7
- [25] K. Fukunaga and L. D. Hostetler. The estimation of the gradient of a density function, with applications in pattern recognition. *IEEE Transactions on Information Theory*, 21:32–40, 1975. 18
- [26] M. Girolami. Mercer kernel-based clustering in feature space. *IEEE Transactions on Neural Networks*, 13(3):780–784, 2002. 4, 5, 13
- [27] M. Hein, T. N. Lal, and O. Bousquet. Hilbertian metrics on probability measures and their application in svms. *Pattern Recognition*, LNCS 3175:270–277, 2004. 4, 7
- [28] D. S. Hochbaum. Polynomial time algorithms for ratio regions and a variant of normalized cut. *IEEE Transactions on Pattern Analysis and Machine Intelligence*, 32(5):889–898, 2010. 6
- [29] T. Hofmann and J. Buhmann. Pairwise data clustering by deterministic annealing. *IEEE Transactions on Pattern Analysis and Machine Intelligence (PAMI)*, 19(1):1–14, January 1997. 6, 9
- [30] Z. Huang. Extensions to the k-means algorithm for clustering large data sets with categorical values. *Data mining and knowledge discovery*, 2(3):283–304, 1998. 8, 19
- [31] S. Jayasumana, R. Hartley, M. Salzmann, H. Li, and M. Harandi. Kernel methods on riemannian manifolds with gaussian rbf kernels. *IEEE Transactions on Pattern Analysis and Machine Intelligence*, In press, 2015. 4
- [32] I. Jermyn and H. Ishikawa. Globally optimal regions and boundaries as minimum ratio weight cycles. *IEEE Transactions on Pattern Analysis and Machine Intelligence (PAMI)*, 23(10):1075–1088, 2001. 6
- [33] M. Kearns, Y. Mansour, and A. Ng. An Information-Theoretic Analysis of Hard and Soft Assignment Methods for Clustering. In *Thirteenth Conference on Uncertainty in Artificial Intelligence (UAI)*, August 1997. 1, 2, 3, 9, 13, 14
- [34] Y. Kee, M. Souiaï, D. Cremers, and J. Kim. Sequential convex relaxation for mutual information-based unsupervised figure-ground segmentation. In *IEEE Conference on Computer Vision and Pattern Recognition (CVPR)*, pages 4082–4089, 2014. 9
- [35] J. Kim, J. W. F. III, A. J. Yezzi, M. Çetin, and A. S. Willsky. A nonparametric statistical method for image segmentation using information theory and curve evolution. *IEEE Transactions on Image Processing*, 14(10):1486–1502, 2005. 9
- [36] V. Kolmogorov, Y. Boykov, and C. Rother. Applications of parametric maxflow in computer vision. In *IEEE International Conference on Computer Vision (ICCV)*, 2007. 6, 12
- [37] B. Kulis, S. Basu, I. Dhillon, and R. Mooney. Semi-supervised graph clustering: a kernel approach. *Machine Learning*, 74(1):1–22, January 2009. 7, 10
- [38] K. Lange, D. R. Hunter, and I. Yang. Optimization transfer using surrogate objective functions. *Journal of Computational and Graphical Statistics*, 9(1):1–20, 2000. 9
- [39] V. Lempitsky, A. Blake, and C. Rother. Image segmentation by branch-and-mincut. In *ECCV*, 2008. 15
- [40] V. Lempitsky, P. Kohli, C. Rother, and T. Sharp. Image segmentation with a bounding box prior. In *Computer Vision, 2009 IEEE 12th International Conference on*, pages 277–284. IEEE, 2009. 16
- [41] T. Li, S. Ma, and M. Ogihara. Entropy-based criterion in categorical clustering. In *International Conference on Machine Learning (ICML)*, 2004. 4
- [42] G. Louppe, L. Wehenkel, A. Suter, and P. Geurts. Understanding variable importances in forests of randomized trees. In *NIPS*, pages 431–439, 2013. 4, 13
- [43] A. Mitiche and I. B. Ayed. *Variational and Level Set Methods in Image Segmentation*. Springer, 2010. 3
- [44] K. Muller, S. Mika, G. Ratsch, K. Tsuda, and B. Schölkopf. An introduction to kernel-based learning algorithms. *IEEE Transactions on Neural Networks*, 12(2):181–201, 2001. 4, 5
- [45] K.-R. Müller, S. Mika, G. Rätsch, K. Tsuda, and B. Schölkopf. An introduction to kernel-based learning algorithms. *IEEE Transactions on Neural Networks*, 12(2):181–201, 2001. 4
- [46] J. Nash. The imbedding problem for riemannian manifolds. *Annals of Mathematics*, 63(1):2063, 1956. 14
- [47] M. S. P. Chan and J. Zien. Spectral k-way ratio cut partitioning. 13:1088–1096, 1994. 8
- [48] S. Paris and F. Durand. A fast approximation of the bilateral filter using a signal processing approach. In *Computer Vision–ECCV 2006*, pages 568–580. Springer, 2006. 15
- [49] V. Roth, J. Laub, M. Kawanabe, and J. Buhmann. Optimal cluster preserving embedding of nonmetric proximity data. *IEEE Transactions on Pattern Analysis and Machine Intelligence (PAMI)*, 25(12):1540–1551, 2003. 5, 6, 7, 8, 10, 11
- [50] C. Rother, V. Kolmogorov, and A. Blake. Grabcut - interactive foreground extraction using iterated graph cuts. In *ACM transactions on Graphics (SIGGRAPH)*, August 2004. 1, 2, 3, 4, 8, 9, 10, 15
- [51] M. Rousson and D. R. A variational framework for active and adaptive segmentation of vector valued images. In *Workshop on Motion and Video Computing*, 2002. 2, 3
- [52] M. B. Salah, A. Mitiche, and I. B. Ayed. Effective level set image segmentation with a kernel induced data term. *IEEE Transactions on Image Processing*, 19(1):220–232, 2010. 2, 8, 9, 19



- [53] B. Schölkopf. The kernel trick for distances. In *Advances in Neural Information Processing Systems (NIPS)*, pages 301–307, 2001. 7
- [54] J. Shi and J. Malik. Normalized cuts and image segmentation. *IEEE Transactions on Pattern Analysis and Machine Intelligence (PAMI)*, 22:888–905, 2000. 5, 6, 8, 9, 10, 11, 12, 14
- [55] K. K. Sung and T. Poggio. Example based learning for view-based human face detection. *IEEE Trans. on Pattern Analysis and Machine Intelligence (TPAMI)*, 20:39–51, 1995. 2, 3
- [56] M. Tang, I. B. Ayed, and Y. Boykov. Pseudo-bound optimization for binary energies. In *European Conference on Computer Vision (ECCV)*, pages 691–707, 2014. 6, 7, 9, 10, 11, 12
- [57] V. Vapnik. *Statistical Learning Theory*. Wiley-Interscience, 1998. 4
- [58] S. Vicente, V. Kolmogorov, and C. Rother. Joint optimization of segmentation and appearance models. In *IEEE International Conference on Computer Vision (ICCV)*, 2009. 12, 15
- [59] S. Wang and J. M. Siskind. Image segmentation with ratio cut. *IEEE Transactions on Pattern Analysis and Machine Intelligence (PAMI)*, 25(6):675–690, 2003. 6
- [60] L. Wasserman. *All of Nonparametric Statistics*. Springer, 2006. 2
- [61] L. Xu, W. Li, and D. Schuurmans. Fast normalized cut with linear constraints. In *IEEE Conference on Computer Vision and Pattern Recognition (CVPR)*, pages 2866–2873, 2009. 7
- [62] S. Yu and J. Shi. Multiclass spectral clustering. In *International Conference on Computer Vision (ICCV)*, 2003. 6, 10, 11
- [63] S. X. Yu and J. Shi. Segmentation given partial grouping constraints. *IEEE Transactions on Pattern Analysis and Machine Intelligence (PAMI)*, 26(2):173–183, 2004. 7
- [64] S. C. Zhu and A. Yuille. Region competition: Unifying snakes, region growing, and Bayes/MDL for multiband image segmentation. *IEEE Transactions on Pattern Analysis and Machine Intelligence*, 18(9):884–900, September 1996. 1, 2, 3, 4, 8, 9